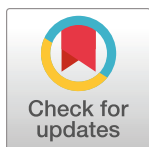


## RESEARCH ARTICLE

## Hybridized distance- and contact-based hierarchical structure modeling for folding soluble and membrane proteins

Rahmatullah Roche<sup>1</sup>, Sutanu Bhattacharya<sup>1</sup>, Debswapna Bhattacharya<sup>1,2\*</sup><sup>1</sup> Department of Computer Science and Software Engineering, Auburn University, Auburn, Alabama, United States of America, <sup>2</sup> Department of Biological Sciences, Auburn University, Auburn, Alabama, United States of America\* [bhattacharyad@auburn.edu](mailto:bhattacharyad@auburn.edu)

## OPEN ACCESS

**Citation:** Roche R, Bhattacharya S, Bhattacharya D (2021) Hybridized distance- and contact-based hierarchical structure modeling for folding soluble and membrane proteins. PLoS Comput Biol 17(2): e1008753. <https://doi.org/10.1371/journal.pcbi.1008753>

**Editor:** Rachel Kolodny, University of Haifa, ISRAEL

**Received:** July 4, 2020

**Accepted:** January 31, 2021

**Published:** February 23, 2021

**Copyright:** © 2021 Roche et al. This is an open access article distributed under the terms of the [Creative Commons Attribution License](https://creativecommons.org/licenses/by/4.0/), which permits unrestricted use, distribution, and reproduction in any medium, provided the original author and source are credited.

**Data Availability Statement:** The FRAGFOLD150 test proteins are available at <http://bioinfadmin.cs.ucl.ac.uk/downloads/>. The CASP12 and CASP13 test proteins are available at <http://predictioncenter.org/>. The membrane protein list is available at <https://data.mendeley.com/datasets/4wht7k4knt/1>. The EVfold test proteins are available at <https://evcouplings.org>. All other data are provided in the paper and the [Supporting Information](#) files.

**Funding:** This work was partially supported by the National Institute of General Medical Sciences [R35GM138146 to DB] and the National Science

## Abstract

Crystallography and NMR system (CNS) is currently a widely used method for fragment-free *ab initio* protein folding from inter-residue distance or contact maps. Despite its widespread use in protein structure prediction, CNS is a decade-old macromolecular structure determination system that was originally developed for solving macromolecular geometry from experimental restraints as opposed to predictive modeling driven by interaction map data. As such, the adaptation of the CNS experimental structure determination protocol for *ab initio* protein folding is intrinsically anomalous that may undermine the folding accuracy of computational protein structure prediction. In this paper, we propose a new CNS-free hierarchical structure modeling method called DConStruct for folding both soluble and membrane proteins driven by distance and contact information. Rigorous experimental validation shows that DConStruct attains much better reconstruction accuracy than CNS when tested with the same input contact map at varying contact thresholds. The hierarchical modeling with iterative self-correction employed in DConStruct scales at a much higher degree of folding accuracy than CNS with the increase in contact thresholds, ultimately approaching near-optimal reconstruction accuracy at higher-thresholded contact maps. The folding accuracy of DConStruct can be further improved by exploiting distance-based hybrid interaction maps at tri-level thresholding, as demonstrated by the better performance of our method in folding free modeling targets from the 12th and 13th rounds of the Critical Assessment of techniques for protein Structure Prediction (CASP) experiments compared to popular CNS- and fragment-based approaches and energy-minimization protocols, some of which even using much finer-grained distance maps than ours. Additional large-scale benchmarking shows that DConStruct can significantly improve the folding accuracy of membrane proteins compared to a CNS-based approach. These results collectively demonstrate the feasibility of greatly improving the accuracy of *ab initio* protein folding by optimally exploiting the information encoded in inter-residue interaction maps beyond what is possible by CNS.

Foundation [IIS-2030722, DBI-1942692 to DB]. The funders had no role in study design, data collection and analysis, decision to publish, or preparation of the manuscript.

**Competing interests:** The authors have declared that no competing interests exist.

## Author summary

Predicting the folded and functional 3-dimensional structure of a protein molecule from its amino acid sequence is of central importance to structural biology. Recently, promising advances have been made in *ab initio* protein folding due to the reasonably accurate estimation of inter-residue interaction maps at increasingly higher resolutions that range from binary contacts to finer-grained distances. Despite the progress in predicting the interaction maps, approaches for turning the residue-residue interactions projected in these maps into their precise spatial positioning heavily rely on a decade-old experimental structure determination protocol that is not suitable for predictive modeling. This paper presents a new hierarchical structure modeling method, DConStruct, which can better exploit the information encoded in the interaction maps at multiple granularities, from binary contact maps to distance-based hybrid maps at tri-level thresholding, for improved *ab initio* folding. Multiple large-scale benchmarking experiments show that our proposed method can substantially improve the folding accuracy for both soluble and membrane proteins compared to state-of-the-art approaches. DConStruct is licensed under the GNU General Public License v3 and freely available at <https://github.com/Bhattacharya-Lab/DConStruct>.

This is a *PLOS Computational Biology* Methods paper.

## Introduction

The development of a computational method that can successfully predict the functional 3-dimensional (3D) structure of a protein molecule purely from its amino acid sequence is of central importance to structural biology [1]. In the recent past, promising progress has been made in this endeavor mediated by reasonably accurate prediction of inter-residue distance or contact maps using sequence co-evolution coupled with deep learning [2–7], and performing data-assisted folding driven by such predicted interaction maps [8–10]. Inter-residue interaction maps contain spatial proximity information that can be translated into geometric constraints to directly construct protein 3D models by maximal constraint satisfaction. Therefore, the prediction of inter-residue distance or contact interaction maps and predicted interaction-assisted 3D structure modeling has fueled considerable research efforts in the community [11,12].

Despite the rapid advances in predicting interaction maps by utilizing state-of-the-art deep learning architectures [4], progress in building 3D models from the predicted maps has been disproportionately slow. ROSETTA molecular modeling suite [13] offers various functions to integrate predicted interaction maps into its internal scoring function as additional constraints for fragment assembly-based *ab initio* folding [14] that can be coupled with loop perturbation sampling [15], but fragment-based folding involves extensive conformational sampling requiring a large amount of computing power. Beyond the realm of time-consuming conformational sampling with fragments, majority of fragment-free distance or contact-based protein folding methods [16–19] rely on a decade-old experimental protein structure determination software called Crystallography and NMR system (CNS) [20], which was originally developed for solving macromolecular geometry from experimental nuclear overhauser enhancement (NOE) restraints as opposed to predicted data and therefore intrinsically incompatible for data-driven

predictive modeling. Even the most recent advances in protein structure prediction [8,9] are primarily due to the progress made in predicting finer-grained interaction maps, but 3D model building from the predicted fine-grained maps still routinely utilize CNS-based experimental structure determination protocol. Because of the dependency on CNS, folding accuracy of computational protein structure modeling methods may get compromised, hindering the realization of their full potential. Thus, there is a critical need to develop a fragment-free folding protocol specifically suitable for predicted inter-residue interaction map data rather than relying on the CNS-based structure determination approach.

CNS-based macromolecular structure determination protocol (CNSsolve) follows several conventions that can be revised for improved folding from predicted inter-residue interaction maps. First, CNS adopts a molecular topology file (.mtf) format for representing polypeptide geometry in all-atom representation, while distance or contact maps are usually defined at a coarse-grained level (e.g., between  $C_\beta$ – $C_\beta$  or  $C_\alpha$ – $C_\alpha$  atom pairs). As such, adaptation of a detailed all-atom representation may not be necessary for distance or contact-assisted folding, at least during the early stages, to accurately predict the backbone geometry while the side-chain atoms can be added conditioned on the backbone conformation subsequently. Adopting a coarse-grained representation reduces the conformational space that may improve folding accuracy and efficiency. Second, CNS has an in-built biophysical force field with bonded and non-bonded terms, some of which may be conflicting or mutually contradictory with the predicted inter-residue interactions, posing difficulties in maximal satisfaction of interaction restraints. Finally, CNS only accepts restraints in a specific format that cannot be easily customized or extended for different applications.

In this article, we present a new inter-residue interaction-assisted hierarchical folding method based on multistage structure modeling with iterative self-correction. Free from the limitations of CNS, our folding method employs 3-stage hierarchical predictive modeling with iterative self-correction driven purely by the geometric restraints induced by inter-residue interactions and secondary structures. Starting from a residue-residue interaction map and secondary structure, our method (DConStruct) can hierarchically estimate the correct overall fold of a target protein in coarse-grained mode to progressively optimize local and non-local interactions while enhancing the secondary structure topology in a self-correcting manner. DConStruct is versatile in that it can exploit the information encoded in the interaction maps at multiple granularities ranging from binary contact maps to distance-based maps at varying thresholds.

We rigorously test DConStruct on several hundred soluble and membrane proteins as well as public data from the latest rounds of the Critical Assessment of techniques for protein Structure Prediction (CASP) experiments. Our experimental results show that DConStruct yields much better folding accuracy than existing CNS-based folding protocols when tested with the same input. Our method attains better performance in folding difficult CASP free modeling targets compared to popular CNS- and fragment-based approaches as well as energy-minimization protocols, some of which even using much finer-grained interaction maps than ours. The open-source DConStruct software package, licensed under the GNU General Public License v3, is freely available at <https://github.com/Bhattacharya-Lab/DConStruct>.

## Results

### DConStruct: hybridized distance- and contact-based hierarchical structure modeling

**Fig 1** illustrates the DConStruct hierarchical structure modeling protocol. Different from the CNS-based approaches [8,9,16–19], DConStruct employs multiscale predictive modeling with iterative self-correction comprising of three modeling stages. The initial modeling stage

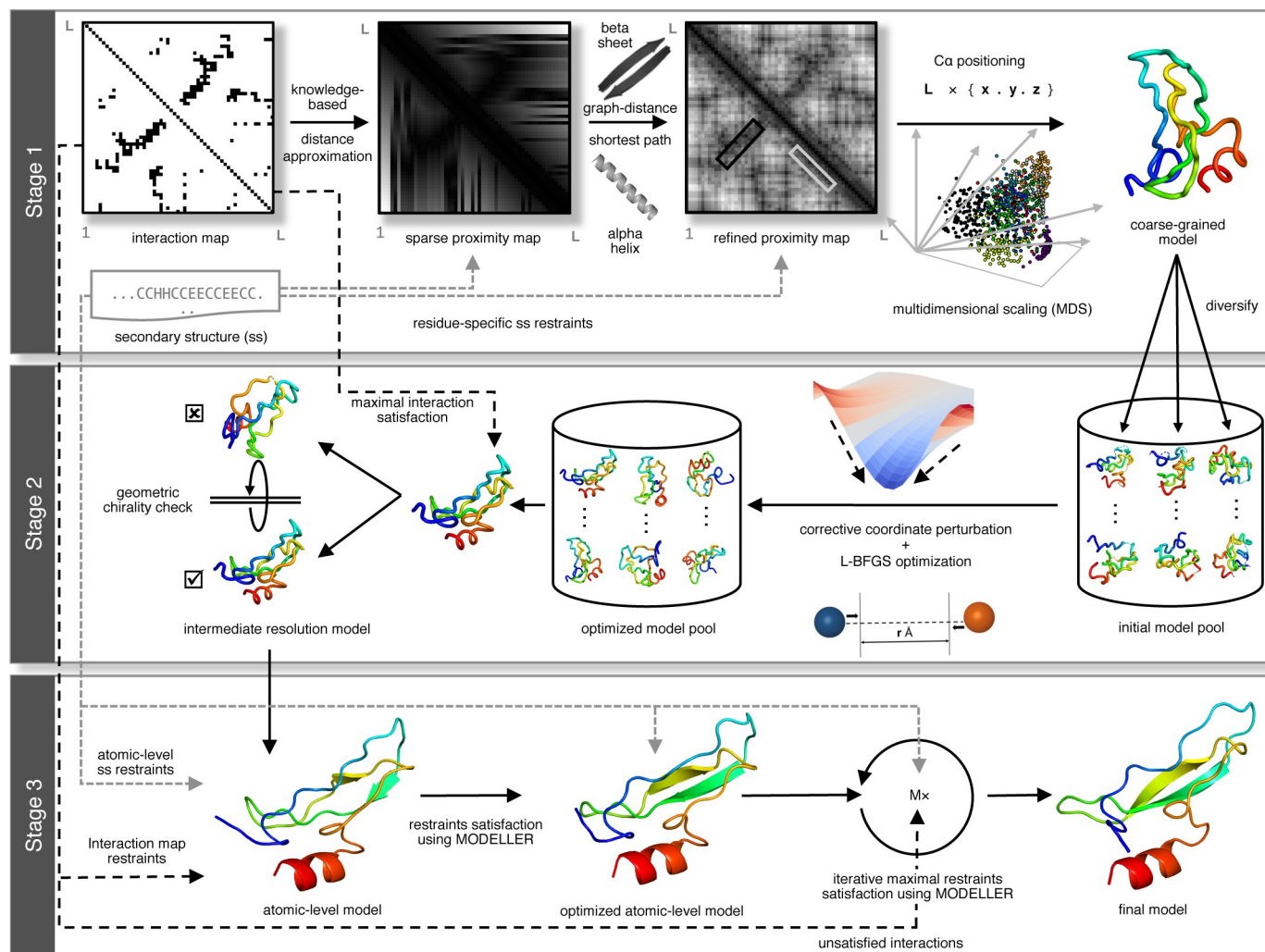


**Fig 1. The 3-stage hierarchical structure modeling protocol of DConStruct.**

<https://doi.org/10.1371/journal.pcbi.1008753.g001>

employs coarse-grained modeling considering the protein conformation as a string of beads, in which each bead corresponds to the  $C_{\alpha}$  atom of an amino acid residue, in order to estimate the overall fold from a sparse set of interatomic interactions and secondary structure information. Given an input interaction map and secondary structure for an amino acid sequence, approximate spatial positioning between the residues is first estimated using prior knowledge of a protein's backbone geometry, derived from the pseudo-covalent bonds formed between the  $C_{\alpha}$  atoms and secondary structure-specific local preferences of the inter-residue distances [21], thus generating a sparse proximity map. For sequentially distant residue pairs, graph-theoretic formulation is adopted to fill the missing entries in the proximity map, which is further refined using the idealized geometry of the secondary structure elements (SSEs) to enhance physical realism. Multidimensional Scaling (MDS) [22–24] is then employed to estimate the 3D coordinates from the proximity map, resulting in a pool of coarse-grained models. The second stage of DConStruct employs iterative self-correction of the coarse-grained model pool using corrective coordinate perturbation heuristics followed by Limited-memory Broyden–Fletcher–Goldfarb–Shanno (LBFGS) [25] optimization. Next, top models are selected based

on maximal satisfaction of the geometric restraints induced by the interaction map coupled with a secondary structure-assisted geometric chirality checking [26]. The final modeling stage of DConStruct consists of atomic-level iterative self-correction. First, MODELLER [27] is used to generate all-atom models from the selected top models. Then, unsatisfied high-confidence interactions, non-interactions, and secondary structure restraints are identified and cumulatively applied with iterative self-correction and model combination to generate the final folded conformation.

Our test data include 150 single domain soluble proteins from the FRAGFOLD dataset [28], 40 Free Modeling (FM) target domains with publicly available experimental structures from the 12th and 13th editions of CASP [29,30], 510 membrane proteins [31,32], and 15 targets from the EVfold set [16]. To evaluate the reconstruction of 3D structural models, we use true residue-residue interaction maps and true secondary structures. To assess *ab initio* folding performance, we use DMPfold [8] and trRosetta [33] distance predictors in conjunction with SPIDER3 [34] secondary structure predictor, all employing cutting-edge deep learning architectures. We install and run DMPfold locally to predict distance histogram maps directly from the multiple sequence alignments (MSA) [35] without using iterative refinement (i.e., rawdistpred.current files) containing 20 distance bins with associated likelihoods between interacting residue pairs. We use a local installation of trRosetta for predicting distance maps from the same multiple sequence alignments (MSA) [35]. We also predict secondary structures by locally installing and running SPIDER3 with default parameter settings. We compare our new method DConStruct against a pure contact-driven approach FT-COMAR [36], CNS-based contact- and secondary structure-driven CONFOLD-like protocols [17,18,31], fragment-based contact- and secondary structure-driven pipelines employing ROSETTA [14,15], CNS-based distance- and secondary structure-driven method DMPfold [8], non-Euclidean distance function-based multi-step modeling approach GDFuzz3D [37], state-of-the-art transform-restrained energy-minimization protocol trRosetta [33], and several top human and server predictors participating in CASP12 and CASP13. For CNS- and ROSETTA-based contact-assisted *ab initio* folding methods [14,18], RaptorX [4] contact maps, obtained by submitting jobs to its web server, are used. CGLFold results are taken directly from its published paper, whereas GDFuzz3D results are obtained by submitting jobs to its web server. All other methods are run locally, as detailed in the Methods section.

## Reconstruction of soluble proteins

We evaluate the reconstruction performance of soluble proteins using the true three-state secondary structures computed from the experimental structures by DSSP [38] and the true  $C_{\alpha}$ - $C_{\alpha}$  and  $C_{\beta}$ - $C_{\beta}$  contact maps calculated at kÅ threshold ( $k = 8, 8.5, 9, 9.5, 10, 10.5, 11, 11.5, 12$ ). We define a contact when the Euclidian distance between two representative atoms ( $C_{\alpha}$ - $C_{\alpha}$  or  $C_{\beta}$ - $C_{\beta}$ ) for a residue pair is at most kÅ with a minimum sequence separation of 6 residues. We compare our new method DConStruct with the standalone contact-based method FT-COMAR [36] and the CNS-based CONFOLD protocol [17] on the 150 FRAGFOLD soluble protein domains with length ranging from 50 to 266 residues. FT-COMAR is a pure distance geometry-based structure reconstruction method that can take only  $C_{\alpha}$ - $C_{\alpha}$  contacts but no secondary structure, whereas CONFOLD is a CNS-based state-of-the-art contact-assisted method that utilizes contact and secondary structure for structure reconstruction. All methods are tested with the same input. The reconstruction accuracy is evaluated for the top predicted models using TM-score [39], a widely used metric for evaluating the quality of 3D structural models.



**Table 1. Reconstruction performance of soluble proteins on 150 FRAGFOLD domains for true  $C_{\alpha}$ - $C_{\alpha}$  contact maps.** The mean TM-score of top predicted models are reported. Values in bold represent the best performance.

Method	8Å	8.5Å	9Å	9.5Å	10Å	10.5Å	11Å	11.5Å	12Å
DConStruct	<b>0.85</b>	<b>0.87</b>	<b>0.9</b>	<b>0.91</b>	<b>0.94</b>	<b>0.95</b>	<b>0.95</b>	<b>0.95</b>	<b>0.95</b>
CONFOLD	0.81	0.82	0.84	0.85	0.86	0.87	0.87	0.88	0.88 <sup>a</sup>
FT-COMAR	0.49	0.51	0.51	0.57	0.62	0.65	0.62	0.65	0.63

<sup>a</sup> CONFOLD fails to run for the target 1dixA at 12Å, and the mean TM-score for CONFOLD is measured over the rest 149 targets at 12Å.

<https://doi.org/10.1371/journal.pcbi.1008753.t001>

As shown in **Tables 1 and 2**, DConStruct significantly outperforms the tested methods FT-COMAR and CONFOLD on the 150 FRAGFOLD soluble protein domains across all thresholds for both  $C_{\alpha}$ - $C_{\alpha}$  (**Table 1**) and  $C_{\beta}$ - $C_{\beta}$  (**Table 2**) contact maps. For the  $C_{\alpha}$ - $C_{\alpha}$  contact maps at the standard threshold of 8Å, the mean TM-score of the top models generated by DConStruct is 0.85, which exceeds that of CONFOLD and FT-COMAR by 0.04 and 0.36 TM-score points, respectively, and statistically significantly better compared to both CONFOLD ( $p$ -value 1.49e-13) and FT-COMAR ( $p$ -value 2.3e-46) at 95% confidence level. Moreover, DConStruct attains a better TM-score than FT-COMAR and CONFOLD for ~99% and ~89% targets, respectively (**S1 Table**). It is interesting to note that for the  $C_{\alpha}$ - $C_{\alpha}$  maps at higher contact thresholds beyond 8Å, in addition to outperforming FT-COMAR by a very large margin, the reconstruction accuracy of DConStruct becomes progressively better compared to CONFOLD as contact threshold increases with DConStruct attaining ~7% (mean TM-scores of 0.90 vs. 0.84), ~9% (mean TM-scores of 0.94 vs. 0.86), and ~9% (mean TM-scores of 0.95 vs. 0.87) better performance compared to CONFOLD at 9, 10, and 11Å contact thresholds, respectively. Between 11Å and 12Å, performance improvement stays at ~9% level with DConStruct attaining a mean TM-score ~0.95, which is much higher than that of CONFOLD (mean TM-score  $\leq$  0.88). **Fig 2A** shows the TM-score distributions of the reconstructed models at various contact thresholds. For all thresholds, the DConStruct distributions are skewed toward higher TM-score regions, indicating better reconstruction performance compared to FT-COMAR and CONFOLD that gets progressively better at higher thresholds. With the increase in contact thresholds, DConStruct results in much more higher number of near-optimal reconstruction cases having TM-score  $\rightarrow$  1.0. For example, at 8 Å threshold, only 3 out of 150 reconstructed models using DConStruct have TM-score  $>$  0.95, whereas CONFOLD fails to reconstruct any structure with TM-score  $>$  0.95. At 12Å threshold, 105 out of 150 (70%) reconstructed models using DConStruct have TM-score  $>$  0.95, whereas CONFOLD attains TM-score  $>$  0.95 only for 11 out of 150 (~7%) cases. Similar trends are observed for the reconstruction with  $C_{\beta}$ - $C_{\beta}$  contact maps, for which DConStruct continues to significantly outperform CONFOLD across all contact thresholds. For the  $C_{\beta}$ - $C_{\beta}$  contact maps at 8Å threshold, DConStruct is statistically significantly better than CONFOLD ( $p$ -value 2.07e-06) and attains better TM-score than CONFOLD for ~73% targets (**S2 Table**). As shown in **Fig 2B**, for  $C_{\beta}$ - $C_{\beta}$

**Table 2. Reconstruction performance of soluble proteins on 150 FRAGFOLD domains for true  $C_{\beta}$ - $C_{\beta}$  contact maps.** The mean TM-score of top predicted models are reported. Values in bold represent the best performance.

Method	8Å	8.5Å	9Å	9.5Å	10Å	10.5Å	11Å	11.5Å	12Å
DConStruct	<b>0.88</b>	<b>0.89</b>	<b>0.90</b>	<b>0.91</b>	<b>0.92</b>	<b>0.93</b>	<b>0.93</b>	<b>0.93</b>	<b>0.93</b>
CONFOLD	0.86	0.87 <sup>a</sup>	0.88	0.89	0.9	0.90 <sup>b</sup>	0.91	0.9	0.9

<sup>a, b</sup> CONFOLD fails to run for target 1smxA at 8.5Å, and for targets 1fcyA, 1ql0A using 10.5Å, and the mean TM-score for CONFOLD is measured over the rest 149 targets at 8.5Å, and over the rest 148 targets at 10.5Å.

<https://doi.org/10.1371/journal.pcbi.1008753.t002>

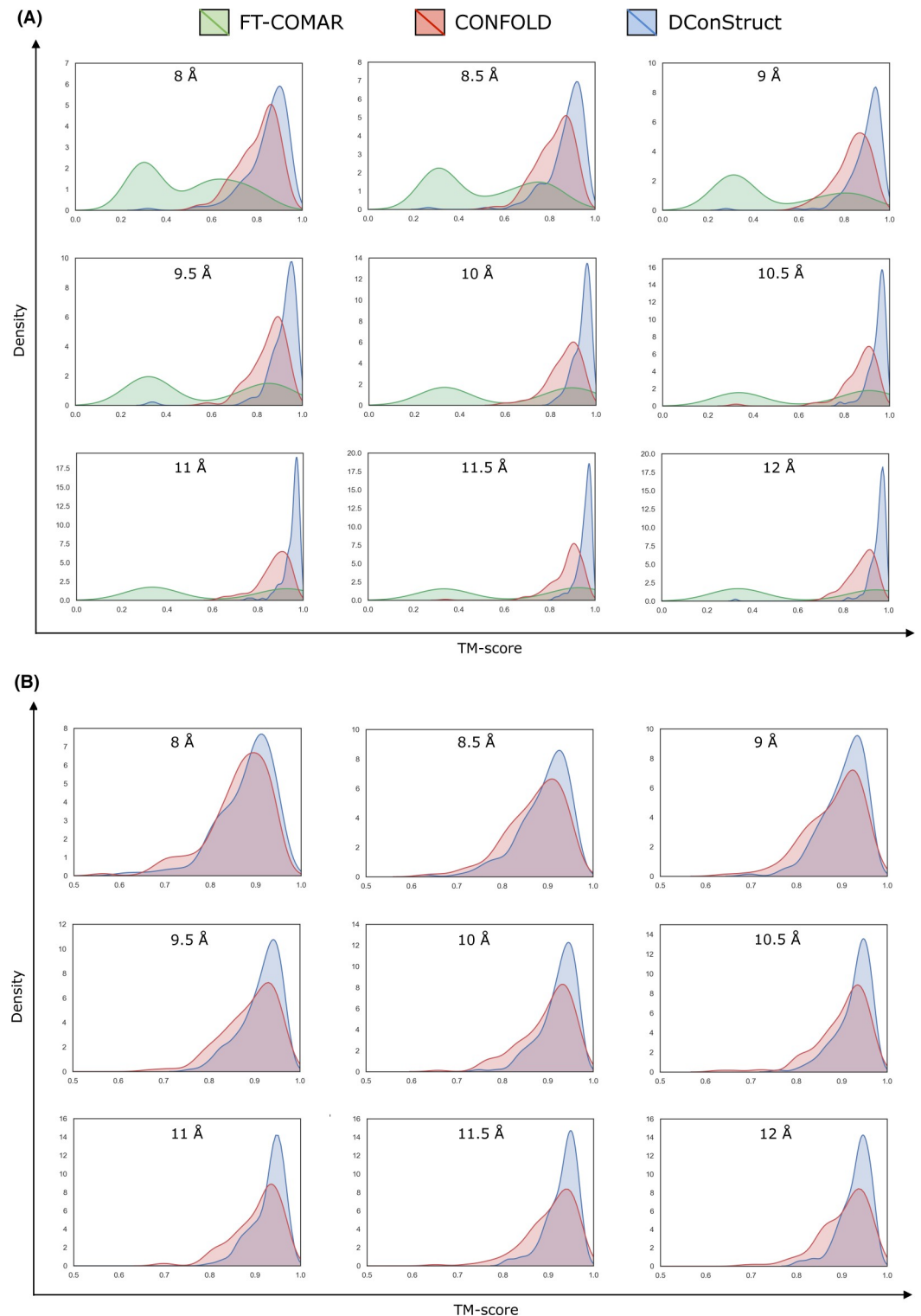


**Fig 2.** TM-score distributions of the reconstructed models on 150 FRAGFOLD soluble protein domains using (A) FT-COMAR, CONFOLD, and DConStruct for true  $C_{\alpha}$ - $C_{\alpha}$  contact maps; and (B) CONFOLD and DConStruct for true  $C_{\beta}$ - $C_{\beta}$  contact maps.

<https://doi.org/10.1371/journal.pcbi.1008753.g002>

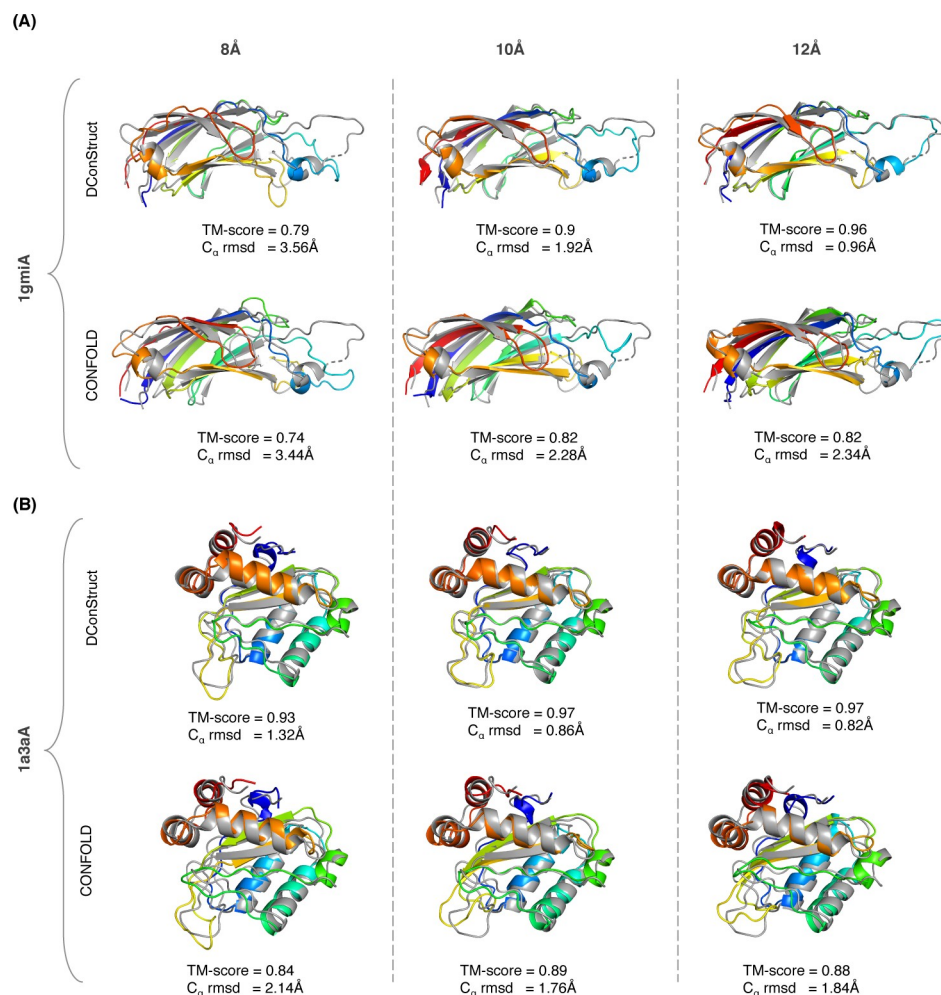


**Fig 3.** Superimpositions between the reconstructed models (rainbow) and the corresponding experimental structures (gray) for two soluble proteins (A) PDB ID 1gmi and chain A; and (B) PDB ID 1a3a and chain A; using DConStruct and CONFOLD for true C<sub>α</sub>-C<sub>α</sub> contact maps at 8, 10, and 12Å thresholds.

<https://doi.org/10.1371/journal.pcbi.1008753.g003>

contacts at higher-thresholded contact maps beyond 8Å, the reconstruction performance of DConStruct gets progressively better compared to CONFOLD with the DConStruct distributions being skewed more and more towards higher TM-score regions. Collectively, the results demonstrate that DConStruct attains much better reconstruction accuracy compared to the CNS-based CONFOLD protocol across multiple contact thresholds for both C<sub>α</sub>-C<sub>α</sub> and C<sub>β</sub>-C<sub>β</sub> contacts in addition to greatly outperforming the pure distance geometry-based FT-COMAR method. Notably, the reconstruction performance of DConStruct becomes markedly better than CONFOLD for higher-thresholded contact maps beyond the standard contact threshold of 8Å currently used by the community. Additional controlled experiments reveal that the better performance of DConStruct at higher-thresholded contact maps is due to the cooperativity between various stages of its hierarchical modeling paradigm, as discussed later.

Two representative examples shown in Fig 3 illustrate the advantage of DConStruct over CNS-based CONFOLD, especially at higher-thresholded contact maps. The first (Fig 3A) is a c2 domain from novel protein kinase C epsilon from Rat (PDB ID: 1gmi), a mainly β protein of 135 residues. For this target, the TM-scores of the reconstructed models using DConStruct



and CONFOLD at 8Å threshold are 0.79 and 0.74, respectively; whereas at 10Å and 12Å thresholds, DConStruct reconstructs much higher quality models with the TM-scores of 0.9 and 0.96, respectively, which are substantially better than CONFOLD having a TM-score of 0.82 at both 10Å and 12Å thresholds. Of note, DConStruct is able to reach sub-angstrom reconstruction accuracy at 12Å threshold for this target with a  $C_\alpha$  root mean squared deviation (rmsd) of 0.96Å, outperforming CONFOLD by a large margin. The second (Fig 3B) is a phosphotransferase IIa-mannitol protein from Escherichia coli (PDB ID: 1a3a). Reconstruction for this  $\alpha+\beta$  target of 145 residues at 8Å threshold results in a TM-score of 0.93 for DConStruct and 0.84 for CONFOLD. At 12Å distance threshold, reconstruction with DConStruct results in a TM-score of 0.97, whereas CONFOLD attains a TM-score of 0.88. Once again, DConStruct reaches sub-angstrom reconstruction accuracy at 12Å threshold with a  $C_\alpha$  rmsd of 0.82Å that is substantially better than CONFOLD.

The results not only demonstrate the advantage of DConStruct over CNS-based CONFOLD, but open up some important follow-up questions. First, recognizing that DConStruct scales at a much better degree of reconstruction accuracy than CONFOLD with the increase in contact thresholds, a natural question to ask is can we improve the performance even further by combining multiple contact thresholds into some form of hybrid interaction maps? Second, does the better reconstruction performance of DConStruct translate to better *ab initio* protein folding? Finally, can we use DConStruct to improve the folding accuracy of membrane proteins? We systematically examine these questions by performing rigorous experiments.

To examine whether it is possible to further improve the reconstruction performance by combining multiple contact thresholds, we formulate hybrid interaction maps at tri-level thresholding. Instead of using a single contact threshold, our hybrid interaction maps use tri-level thresholding with variable upper bounds of 8, 10, and 12Å derived from the Euclidian distance between two representative atoms ( $C_\alpha-C_\alpha$  or  $C_\beta-C_\beta$ ) for a residue pair having a minimum sequence separation of 6 residues. That is, we interpolate the real-valued Euclidian distance between a residue pair to one of the three upper bounds, thus resulting in tri-level thresholding. We reconstruct the same set of 150 soluble proteins after feeding the hybrid interaction maps and three-state secondary structures into DConStruct, and compute the TM-scores of the reconstructed models.

For the  $C_\alpha-C_\alpha$  maps, running DConStruct with the hybrid interaction maps results in near-optimal reconstruction with a mean TM-score of 0.97, which not only outperforms the mean TM-score of reconstruction with binary contact maps across all thresholds but also yields better TM-scores for 149 out of 150 (~99%) cases than 8 and 10Å thresholds and 144 out of 150 (~96%) cases than 12Å threshold (S3 Table). For the  $C_\beta-C_\beta$  maps, reconstruction with the hybrid interaction maps leads to better TM-scores than reconstruction with binary contact maps for 145 out of 150 (~97%), 99 out of 150 (~66%), and 87 out of 150 (~58%) cases for 8, 10, and 12Å thresholds, respectively (S4 Table). That is, DConStruct with hybrid interaction maps at tri-level thresholding yields better reconstruction performance than contact maps at a fixed threshold. As shown in Fig 4, running DConStruct with hybrid maps further improves the reconstruction accuracy for the two representative proteins described in Fig 3 with the first protein (PDB ID: 1gmi) attaining a TM-score of 0.97 and the second protein (PDB ID: 1a3a) achieving a TM-score of 0.98, both reaching improved sub-angstrom  $C_\alpha$  rmsds of 0.78Å and 0.62Å for 1gmi and 1a3a, respectively.

## Folding CASP free modeling targets

To investigate whether the improved reconstruction performance of DConStruct translates to better *ab initio* folding, we perform predictive modeling for 40 free modeling (FM) targets

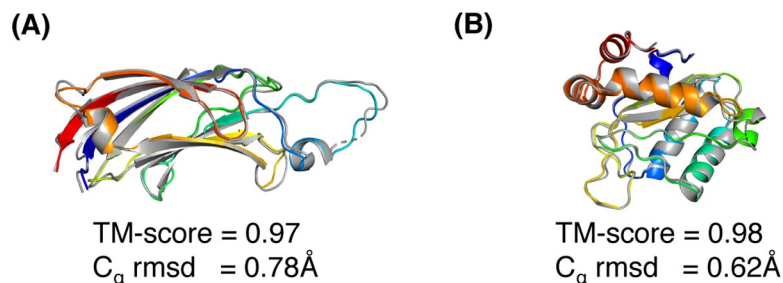


**Fig 4.** Superimpositions between the reconstruction models (rainbow) and its native structure (gray) for two soluble proteins (A) PDB ID 1gmi and chain A; and (B) PDB ID 1a3a and chain A; generated by DConStruct with hybrid interaction maps at tri-level thresholding.

<https://doi.org/10.1371/journal.pcbi.1008753.g004>

with publicly available experimental structures from the 12th and 13th rounds of the Critical Assessment of techniques for protein Structure Prediction (CASP) experiments. We compare the predictive modeling performance of DConStruct with two CNS-based approaches: DMPfold [8] and CONFOLD2 [18], as well as two fragment-based methods: ROSETTA [13] as used in the PConsFold protocol [14] and CGLfold [15]. We also compare DConStruct with GDFuzz3D [37], a multi-step protocol that uses a non-Euclidean distance function. DMPfold [8] is a cutting-edge *ab initio* folding method that employs deep learning to predict inter-atomic distance bounds, torsion angles, and hydrogen bonds and feeds these constraints into CNS to build models in an iterative fashion. CONFOLD2 [18] employs CNS to integrate predicted contacts and secondary structure in a two-stage modeling pipeline in which unsatisfied contacts are filtered out after initial model generation. Popular fragment-based method ROSETTA [13] adds constraints from predicted contacts into the well-established fragment assembly engine as implemented in the PconsFold [14] protocol. CGLfold [15] is a recent fragment-based method that combines global exploration and loop perturbation using predicted contacts. GDFuzz3D [37] employs multi-step modeling that involves a combination of coarse-grained and all-atom modeling. We run DMPfold with default parameter settings to predict structural models using its CNS-based iterative modeling. CONFOLD2 only accepts contact maps at 8 Å threshold and PconsFold protocol utilizes ROSETTA's FADE function for contact constraints with its parameters set for 8 Å contacts. We, therefore, perform *ab initio* folding using CONFOLD2 and ROSETTA by feeding 8 Å contact maps predicted from the state-of-the-art RaptorX contact prediction method [4] together with secondary structures predicted using SPIDER3 [34]. For CGLFold, we collect results for the 29 CASP FM targets from their published paper [15]. For GDFuzz3D, we submit jobs to its web server, which is limited to protein size of less than 400 residues. A total of 28 CASP FM domains have length less than 400 residues and we obtain the GDFuzz3D predicted models for these targets by feeding the RaptorX predicted contacts to its web server. To perform predictive modeling using DConStruct driven by hybrid interaction maps at tri-level thresholding, we collect the DMPfold predicted initial distance histograms (rawdispred.current files) containing 20 distance bins with associated likelihoods and convert them into hybrid interaction maps with variable upper bounds of 8, 10, and 12 Å by summing up the likelihoods for distance bins below the three distance thresholds of 8, 10, and 12 Å and subsequently select the top contacts based on their likelihoods, resulting in predicted hybrid interaction maps at tri-level thresholding. In addition to predicted hybrid interaction maps, we also feed three-state secondary structures predicted using SPIDER3 [34] into DConStruct. Unlike DMPfold, we do not use any other predicted structural features such as torsion angles and hydrogen bonds or perform any CNS-based iterative modeling in DConStruct. To evaluate *ab initio* folding performance, we compare TM-

**Table 3. Folding performance of CASP free modeling protein targets on 40 CASP12 and CASP13 free modeling target domains.** Values in bold represent the best performance.

Method	Mean TM-score	Median TM-score	# TM-scores > 0.5
DConStruct	<b>0.46</b>	<b>0.50</b>	<b>20/40</b>
DMPfold	0.42	0.38	15/40
GDFuzz3D <sup>a</sup>	0.41	0.39	9/28
CGLFold <sup>b</sup>	0.40	0.43	8/29
CONFOLD2	0.38	0.32	10/40
ROSETTA	0.37	0.36	6/40

<sup>a</sup> GDFuzz3D results are reported for 28 CASP free modeling target domains having length less than 400 residues, obtained by submitting jobs to its web server, which is limited to protein target residues less than 400 residues.

<sup>b</sup> CGLFold results are adopted directly from the published results containing 29 CASP free modeling target domains.

<https://doi.org/10.1371/journal.pcbi.1008753.t003>

scores of the top predicted models from each of the tested methods. Additionally, we evaluate the number of models with correct overall folds having TM-score > 0.5 [40].

As reported in **Table 3**, DConStruct outperforms all other methods by attaining better TM-scores and correctly folding more FM targets. DConStruct attains the highest mean TM-score of 0.46, which is statistically significantly better than the second-best performing method DMPfold (mean TM-score of 0.42) at 95% confidence level ( $p$ -value of 0.03329857). The median TM-score of DConStruct is 0.5, which is also the highest and significantly better than all competing methods, including the CNS-based protocols DMPfold and CONFOLD2 as well as the fragment-based approaches ROSETTA and CGLFold (**S5 Table**). DConStruct correctly folds 20 out of 40 CASP FM targets, whereas the number of correct folds for DMPfold, CONFOLD2, CGLFold, ROSETTA, and GDFuzz3D are only 15, 10, 8, 6, and 9, respectively. Of note, when compared head-to-head with CGLFold (**S6 Table**) and GDFuzz3D (**S7 Table**) on the common set of targets comprising of 29 and 28 CASP FM targets for CGLFold and GDFuzz3D, respectively, the performance of DConStruct is even better with a mean TM-score of 0.49 and a median TM-score > 0.5 in both cases. We also compare DConStruct with a customized version of DMPfold by changing its input interface to use the same multiple sequence alignments [35] as used in DConStruct. While the customized version of DMPfold leads to better performance over the default DMPfold method by improving the mean and median TM-scores to 0.44 and 0.43, respectively (**S8 Table**), DConStruct still outperforms (mean TM-score of 0.46 and median TM-score of 0.5) the customized version of DMPfold, let alone the default DMPfold method. The results demonstrate that DConStruct delivers much better *ab initio* folding performance compared to the CNS- and fragment-based approaches, including the state-of-the-art DMPfold protocol employing CNS-based iterative modeling using much finer-grained distance maps than ours together with additional predicted structural features such as torsion angles and hydrogen bonds. Of note, the hybrid interaction maps used in DConStruct are derived from the DMPfold predicted initial distance histograms. That is, even with lower-resolution interaction maps and much less information, DConStruct leads to better *ab initio* folding accuracy than CNS, underscoring its effectiveness in predictive modeling with inter-residue interaction maps beyond what is possible by CNS.

**Fig 5** shows the *ab initio* models predicted by DMPfold and DConStruct for four representative CASP FM targets. For the two CASP12 FM targets T0898-D1 and T0870-D1, DMPfold fails to attain the correct overall fold whereas DConStruct correctly folds both targets attaining TM-scores of 0.65 and 0.67 for T0898-D1 and T0870-D1, respectively. T0968s2-D1 and T0957s2-D1 are two CASP13 FM targets, for both of which DConStruct predicts more

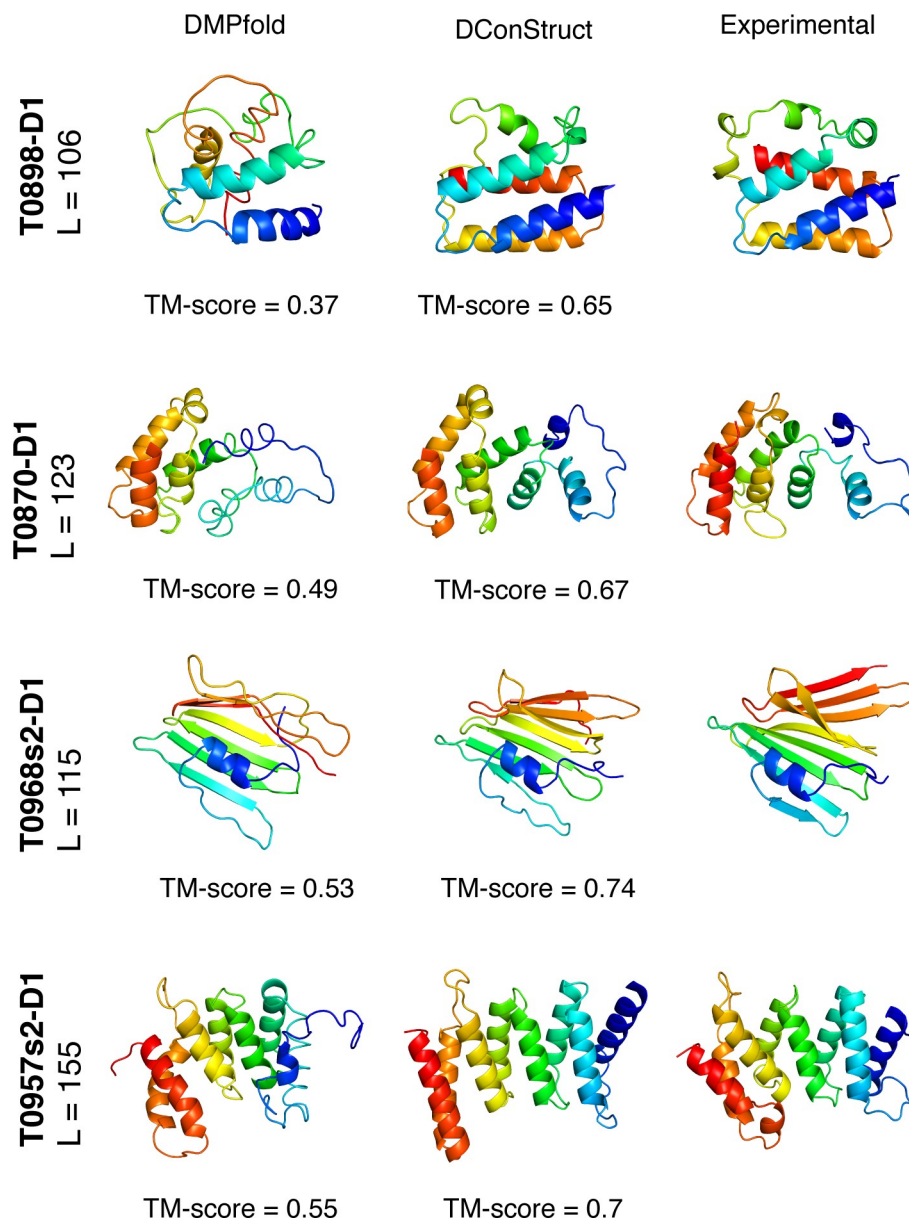


**Fig 5. Ribbon diagrams of 3D models for the four CASP FM targets: T0898-D1, T0870-D1, T0968s2-D1, and T0957s2-D1; predicted by DMPfold and DConStruct along with the experimental structures.** All molecules are rainbow colored blue to red from the N- to C-termini. Models are optimally superimposed on the experimental structures, and then separated by translations along the horizontal direction.

<https://doi.org/10.1371/journal.pcbi.1008753.g005>

accurate models with TM-score  $\geq 0.7$ , much better than DMPfold. In summary, the advantage of DConStruct over the state-of-the-art CNS-based *ab initio* folding method DMPfold is significant.

A salient feature of DConStruct is its flexibility to use distance maps predicted by any method, not just DMPfold. To demonstrate such versatility, we integrate DConStruct with trRosetta [33] to perform *ab initio* folding for the 40 CASP FM targets. trRosetta is a state-of-the-art deep learning-based protein structure prediction method that predicts inter-residue distances and orientation (dihedral and planar angles). The predicted angles and distances are

**Table 4. Folding performance of DConStruct using trRosetta-predicted distance maps compared to top CASP predictors and trRosetta distance-only modeling on 40 CASP12 and CASP13 free modeling target domains.**

Method	Mean TM-score	Median TM-score	# TM-scores > 0.5
A7D <sup>a</sup>	0.60	0.61	12/17
DConStruct (with trRosetta distance maps)	0.49	0.51	21/40
Zhang <sup>b</sup>	0.44	0.44	12/39
BAKER <sup>b</sup>	0.43	0.41	13/39
trRosetta (distance-only)	0.42	0.34	12/40
MULTICOM <sup>b</sup>	0.42	0.4	10/39
Zhang-Server	0.41	0.42	12/40
Jones-UCL <sup>b, c</sup>	0.39	0.37	10/38
RaptorX-Contact	0.38	0.35	9/40
BAKER-ROSETTASERVER	0.35	0.34	4/40

<sup>a</sup> A7D results contain only 17 CASP13 free modeling target domains.

<sup>b</sup> CASP human groups' results do not include the server-only target T0950-D1.

<sup>c</sup> Jones-UCL results additionally do not include the target T0869-D1 due to missed submission.

<https://doi.org/10.1371/journal.pcbi.1008753.t004>

subsequently transformed to ROSETTA restraints to generate 3D structures through ROSETTA energy-minimization protocol [13]. We collect the trRosetta-predicted distance maps for the 40 CASP FM targets using the same multiple sequence alignments [35] previously indicated and convert them into hybrid interaction maps at tri-level thresholding to feed them into DConStruct along with SPIDER3-predicted secondary structures. Since trRosetta-based modeling uses both distance and orientation information whereas DConStruct is a hybridized distance- and contact-based method, we employ trRosetta-based modeling using only distance information for a fair performance comparison with DConStruct-based modeling that uses the same trRosetta distance maps, albeit at tri-level thresholding. We run trRosetta-based modeling locally with the parameter setting ('--no-orient') that uses the fine-grained distance information predicted from trRosetta but no orientation information. Additionally, we compare the performance of DConStruct-based modeling with trRosetta distance maps with the top performing predictors (server and human groups) participating in both CASP12 and CASP13 experiments including A7D, RaptorX-Contact, BAKER-ROSETTASERVER, BAKER, Zhang-Server, Zhang, Jones-UCL, and MULTICOM [29,30] by collecting the TM-scores of the top CASP predictors directly from the CASP website (S8 Table). As shown in Table 4, the integration of with DConStruct with trRosetta improves the performance even further, attaining a mean TM-score of 0.49 and a median TM-score of 0.51 with 21 correct folds, significantly better than the distance-only trRosetta-based modeling having a mean TM-score of 0.42 and a median TM-score of 0.34 with only 12 correct folds. When compared to the top CASP predictors, DConStruct with trRosetta outperforms all other methods except A7D, the CASP13-winning AlphaFold [41] method, even though A7D results are based only on a small subset of 17 CASP13 FM targets as A7D (or AlphaFold) did not participate in CASP12. Compared to the top CASP predictors participating in both CASP12 and CASP13, many of which exploit template and/or fragment information along with additional manual interventions possibly for some of the human groups, DConStruct with trRosetta attains much better performance. Fig 6 shows the models predicted by RaptorX-Contact, BAKER, Zhang, A7D, trRosetta distance-only modeling, and DConStruct using trRosetta-predicted distance maps for three large CASP FM targets (length > 245). The top CASP predictors fail to attain the correct overall fold for the CASP12 FM targets T0864-D1 and T0904-D1, whereas DConStruct correctly folds both targets attaining TM-scores of 0.73, and 0.77 respectively. While



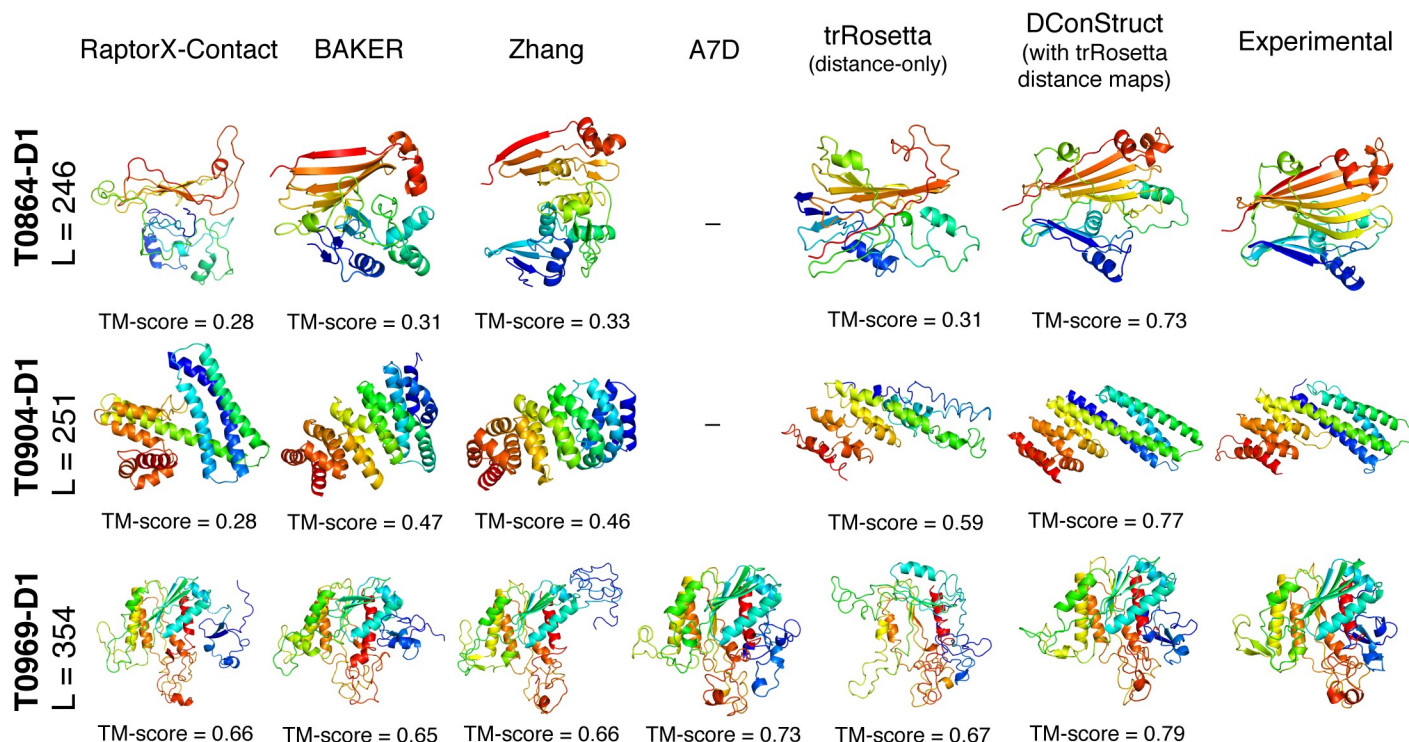


**Fig 6. Ribbon diagrams of 3D models for the three CASP FM large targets: T0864-D1, T0904-D1, and T0969-D1; predicted by the top CASP human and server predictors, trRosetta distance-only modeling, and DConStruct using trRosetta-predicted distance maps along with the experimental structures. A7D prediction is relevant only for CASP13 target T0969-D1. All molecules are rainbow colored blue to red from the N- to C-termini. Models are optimally superimposed on the experimental structures, and then separated by translations along the horizontal direction.**

<https://doi.org/10.1371/journal.pcbi.1008753.g006>

trRosetta distance-only modeling attains correct fold for T0904-D1 (TM-score 0.59), one of the two CASP12 FM targets, the folding performance is much lower than DConStruct. For the CASP13 large FM target T0969-D1, DConStruct predicts accurate 3D model (TM-score of 0.79), which is better than the top CASP predictors including the AlphaFold method employed in A7D (TM-score of 0.73) as well as trRosetta distance-only modeling (TM-score of 0.67). The results indicate that DConStruct is versatile in that it can be seamlessly integrated with trRosetta to perform hybridized distance- and contact-based modeling, while attaining state-of-the-art performance.

One may argue that DConStruct achieves better folding performance than several other approaches simply because the hybrid interaction maps fed into DConStruct are of higher quality containing more fine-grained information. This is not true when we look at the performance comparison of DConStruct to the customized version of DMPfold employing CNS-based modeling and distance-only trRosetta-based energy-minimization. On 40 CASP12 and CASP13 free modeling target domains, DConStruct attains better folding performance with a mean TM-score of 0.46 and a median TM-score of 0.5 compared to the customized version of DMPfold having a mean TM-score of 0.44 and a median TM-score of 0.43 (S8 Table). While both DConStruct and the customized version of DMPfold pipeline perform 3D folding based on the same original distance maps predicted by DMPfold from the same multiple sequence alignments [35], the CNS-based iterative modeling used in the customized version of DMPfold pipeline uses much finer-grained distance maps than ours together with additional predicted structural features such as torsion angles and hydrogen bonds. That is, the 3D folding protocol employed by DConStruct is the primary driver of its improved performance, even when using

much less information. Similarly, DConStruct achieves much better performance with a mean TM-score of 0.49 and a median TM-score of 0.51 compared to trRosetta-based energy-minimization having a mean TM-score of 0.42 and a median TM-score of 0.34 (Table 4). Once again, both DConStruct and energy-minimization-based folding protocols use the original distance maps predicted by trRosetta from the same multiple sequence alignments, but trRosetta-based energy-minimization protocol utilizes the full-fledged distance histograms containing much finer-grained information whereas DConStruct uses hybrid interaction maps at tri-level thresholding derived from the original distance histograms. In summary, DConStruct-based folding leads to better 3D models than CNS- and energy-minimization-based methods.

## Folding membrane proteins

Membrane proteins (MPs) have significant therapeutic values because of their importance in drug design [42]. However, only a small fraction of MPs are amenable to homology modeling, partially due to the lack of sufficient MPs with experimentally solved structures. Recently, the Xu group has developed a deep transfer learning (DTL) method for predicting the interaction maps from the sequences of the MPs that can be fed into CNS-based *ab initio* folding to predict the 3D structure of the MPs. The method (hereafter called Xu's DTL with CNS) has demonstrated state-of-the-art performance on a dataset of 510 non-redundant MPs [31]. Noticing the ability of DConStruct to achieve improved *ab initio* folding accuracy for CASP FM targets, we examine whether DConStruct can improve *ab initio* folding accuracy of the MPs by exploiting distance-based hybrid interaction maps. For the 510 MPs, we follow the same protocol adopted for *ab initio* folding of CASP FM targets by obtaining the hybrid interaction maps from DMPfold- and trRosetta-predicted distance maps and feeding them independently to DConStruct along with SPIDER3 predicted secondary structures for predicting the 3D structures of the MPs. We collect the top predicted 3D models using Xu's DTL with CNS from the Mendeley Data provided in the published paper [31] to directly compare with DConStruct. As shown in Table 5, using DMPfold-predicted distance maps, DConStruct attains an improved mean TM-score of 0.55, which is higher than Xu's DTL with CNS (mean TM-score of 0.52). The performance of DConStruct is even better (mean TM-score of 0.59) when trRosetta-predicted distance maps are used. For DConStruct using DMPfold- and trRosetta-predicted distance maps, the TM-scores have a median of 0.54 and 0.61, respectively, better than that of Xu's DTL with CNS having a median TM-score of 0.5. The performance of DConStruct is statistically significantly better at 95% confidence level ( $p$ -value =  $6.54 \times 10^{-6}$  for DConStruct with DMPfold-predicted distance maps,  $p$ -value =  $5.11 \times 10^{-27}$  for DConStruct with trRosetta-predicted distance maps). Furthermore, DConStruct using DMPfold-predicted distance maps correctly folds 294 MP targets with a success rate of ~58%, which is ~8% higher than the success rate of Xu's DTL with CNS (50%) that can fold only 255 MP targets correctly (S9 Table). When trRosetta-predicted distance maps are used by DConStruct, the success rate reaches to ~67% (correctly folds 342 MP targets), which is 17% higher than Xu's DTL with CNS (S9 Table). The results confirm that DConStruct leads to improved *ab initio* folding accuracy even

**Table 5. Folding performance of 510 MPs using Xu's deep transfer learning (DTL) with CNS and DConStruct.** Values in bold represent the best performance.

Method	Mean TM-scores	Median TM-score	# TM-score > 0.5
DConStruct (with trRosetta distance maps)	<b>0.59</b>	<b>0.61</b>	<b>342/510</b>
DConStruct (with DMPfold distance maps)	0.55	0.54	294/510
Xu's DTL with CNS	0.52	0.50	255/510

<https://doi.org/10.1371/journal.pcbi.1008753.t005>

for MPs while underscoring the versatility of DConStruct to utilize distance information predicted by different methods.

**Fig 7** shows the 3D models predicted by Xu's DTL with CNS and DConStruct (using DMPfold- and trRosetta-predicted distance maps) for five MPs with lengths varying from 210 to 534 residues. For all five targets, DConStruct predicts correct overall fold attaining a TM-score of at least 0.7 and reaching as high as 0.84 TM-score for the target 4g1uA, whereas the Xu's DTL with CNS fails to correctly fold any of the targets having a maximum TM-score of only 0.47.

### The three stages of DConStruct and their implications in hierarchical protein folding

To evaluate the relative contributions of the three stages adopted in DConStruct hierarchical structure modeling, we perform stage-by-stage 3D reconstruction of 15 protein targets tested in EVfold [16] and study their folding accuracy and correctness of secondary structure topology. For each protein, we use the true three-state secondary structure computed from the experimental structures using DSSP [38] and the true  $C_{\beta}$ - $C_{\beta}$  contact maps calculated at 8Å threshold having a minimum sequence separation of 6 residues. The rationale for using true input information is to prevent any bias caused by possible prediction noise in stage-wise hierarchical folding. In addition to measuring the stagewise folding accuracy using TM-score, we compute the percentage of correctly recovered secondary structure topology for the helix ( $Q_H$ ) and beta strand ( $Q_E$ ) residues.

As reported in **Table 6**, the mean TM-score after employing only stage 1 is 0.54 and 6 out of 15 targets fail to attain correct overall fold with poor secondary structure topology having a mean  $Q_H$  of ~13% and a mean  $Q_E$  of only ~1%. By introducing stage 2, the mean TM-score significantly improves to 0.76 with all proteins attaining correct overall folds. There is also a marked improvement in the helix topology having a mean  $Q_H$  of ~59%, although beta strand topology still remains suboptimal at a mean  $Q_E$  of ~13%. Stage 3 further improves the folding accuracy, attaining a mean TM-score of 0.83 but it is not as pronounced as the difference between stage 2 and stage 1. Much better mean  $Q_H$  of ~94% is achieved with the introduction of stage 3, indicating near-optimal helix topology along with substantial improvement in beta strand topology having a mean  $Q_E$  of ~62%. The results offer some interesting insights. First, as shown in **Fig 8**, the folding accuracy gain is substantial with the introduction of stage 2 with the TM-score distributions getting shifted to higher accuracy regions (0.22 mean TM-score gain from stage 1) compared to stage 3 (only 0.08 mean TM-score gain from stage 2), indicating that iterative self-correction with local structural perturbation is very effective in improving the overall fold-level accuracy. Second, stage 2 not only greatly improves the overall fold but also facilitates the formation of short-range hydrogen bonds, as demonstrated by significantly higher mean  $Q_H$  compared to stage 1. Third, while stage 3 has only minor contribution in boosting the overall fold-level accuracy, it optimizes the secondary structure topology through iterative self-correction by facilitating long-range hydrogen bonds formation for stabilizing the beta sheet geometry as revealed by much higher mean  $Q_E$  in addition to attaining near-optimal short-range hydrogen bonds by reaching close-to-optimal mean  $Q_H$ . We note that the final mean  $Q_E$  is still far from optimal, indicating that there is room for improvement in accurately modeling the beta strands. In summary, the three stages of the hierarchical structure modeling adopted in DConStruct have complementary roles. Stage 2 is primarily responsible for improving the global folding accuracy beyond what can be achieved by the coarse-grained modeling in stage 1, whereas stage 3 is responsible for the refinement of global fold

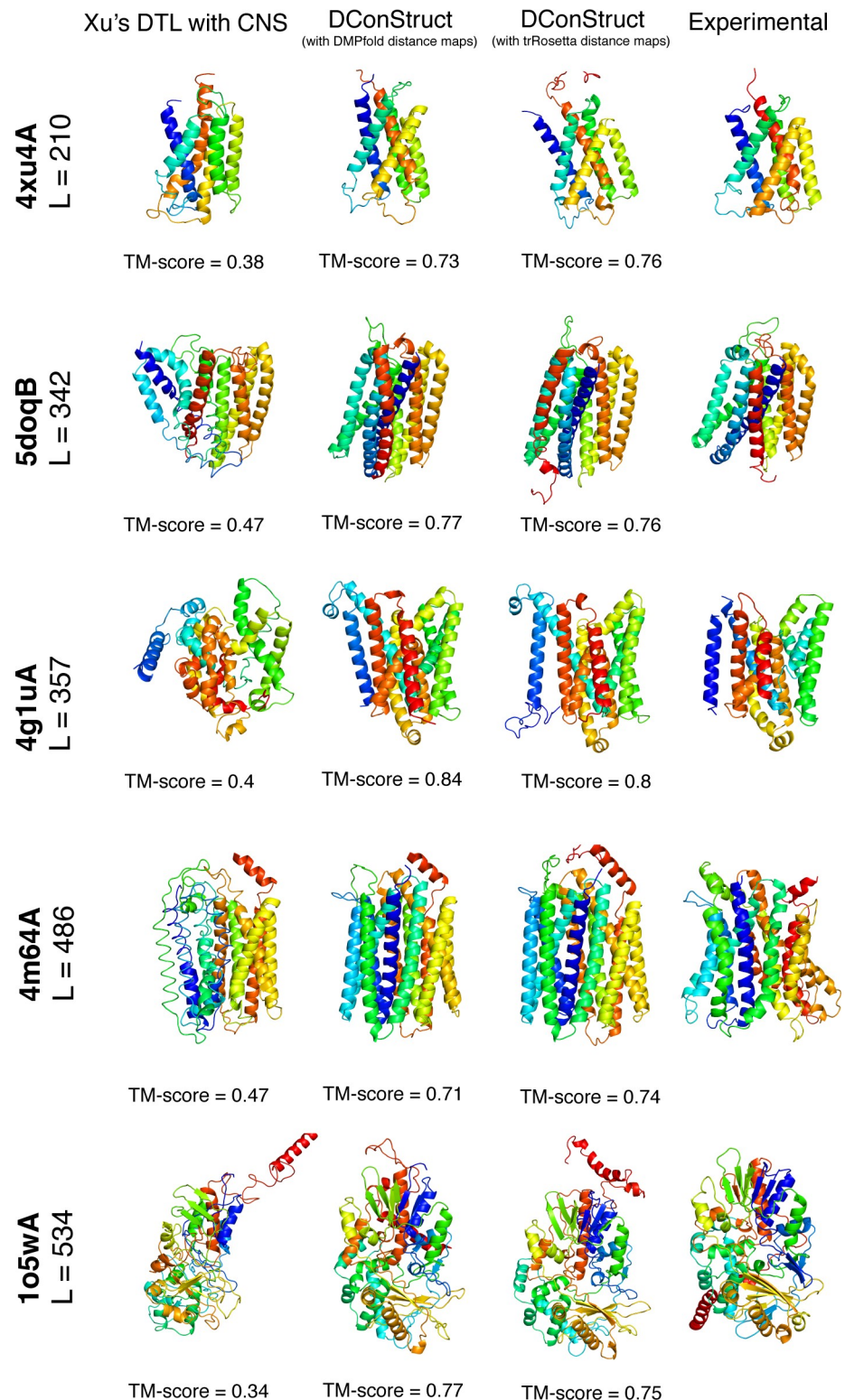


**Fig 7. Ribbon diagrams of 3D models of MPs predicted using Xu's DTL with CNS and DConStruct (using DMPfold- and trRosetta-predicted distance maps) along with the experimental structures for five protein targets: PDB ID 4xu4 and chain A, PDB ID 5doq and chain B, PDB ID 4g1u and chain A, PDB ID 4m64 and chain A, and PDB ID 1o5w and chain A.** All molecules are rainbow-colored blue to red from the N- to C-termini. Models are optimally superimposed on the experimental structures and then separated by translations along the horizontal direction.

<https://doi.org/10.1371/journal.pcbi.1008753.g007>



**Table 6. Stage-by-stage 3D reconstruction results for 15 protein targets in EVfold dataset using true  $C_{\beta}$ - $C_{\beta}$  contact maps at 8Å threshold and true secondary structures<sup>a</sup>.**

Target	Stage 1			Stage 1 + Stage 2			Stage 1 + Stage 2 + Stage 3		
	TM-score	Q <sub>H</sub>	Q <sub>E</sub>	TM-score	Q <sub>H</sub>	Q <sub>E</sub>	TM-score	Q <sub>H</sub>	Q <sub>E</sub>
1bkrA	0.75	37.14	-	0.87	74.29	-	0.90	98.57	-
1e6kA	0.61	37.25	0.00	0.79	70.59	20.00	0.87	92.16	85.00
1f21A	0.65	29.31	4.17	0.82	63.79	27.08	0.88	98.28	60.42
1g2eA	0.43	14.29	0.00	0.67	80.95	0.00	0.77	100.00	36.00
1hzxA	0.75	1.1	0.00	0.87	60.22	0.00	0.91	86.19	25.00
1oddA	0.60	9.38	0.00	0.67	59.38	0.00	0.77	100.00	42.86
1r9hA	0.44	0.00	0.00	0.74	42.86	0.00	0.82	100.00	77.78
1rqmA	0.59	10.26	0.00	0.80	51.28	24.00	0.84	89.74	68.00
1wvnA	0.45	19.36	0.00	0.71	74.19	17.65	0.78	100.00	70.59
2hdaA	0.24	-	5.26	0.53	-	0.00	0.61	-	47.37
2it6A	0.52	11.11	0.00	0.79	66.67	8.82	0.86	100.00	58.82
2o72A	0.38	-	2.13	0.71	-	27.66	0.81	-	87.23
3tgiE	0.64	0.00	2.63	0.88	0.00	13.16	0.94	57.14	71.05
5p21A	0.61	0.00	0.00	0.88	75.81	5.13	0.93	98.39	74.36
5ptiA	0.44	0.00	0.00	0.64	50.00	40.00	0.79	100.00	60.00
<b>Mean</b>	<b>0.54</b>	<b>13.02</b>	<b>1.01</b>	<b>0.76</b>	<b>59.23</b>	<b>13.11</b>	<b>0.83</b>	<b>93.88</b>	<b>61.75</b>

<sup>a</sup> For target 1bkrA, Q<sub>E</sub> scores are ignored since there is no beta strand residue in the experimental structure; and for targets 2hdaA and 2o72A, Q<sub>H</sub> scores are ignored since there are no helix residues in their experimental structures.

<https://doi.org/10.1371/journal.pcbi.1008753.t006>

while stabilizing the local secondary structure topology. All three stages, working cooperatively in a hierarchical manner, contribute to enhancing 3D folding at both global and local levels.

A representative example from the EVfold dataset shown in Fig 9 may help further elucidate the relative contributions of the three stages used in DConStruct. This is an  $\alpha/\beta$  protein of 165 residues (PDB ID: 5p21 chain A). While stage 1 is able to attain the correct overall fold

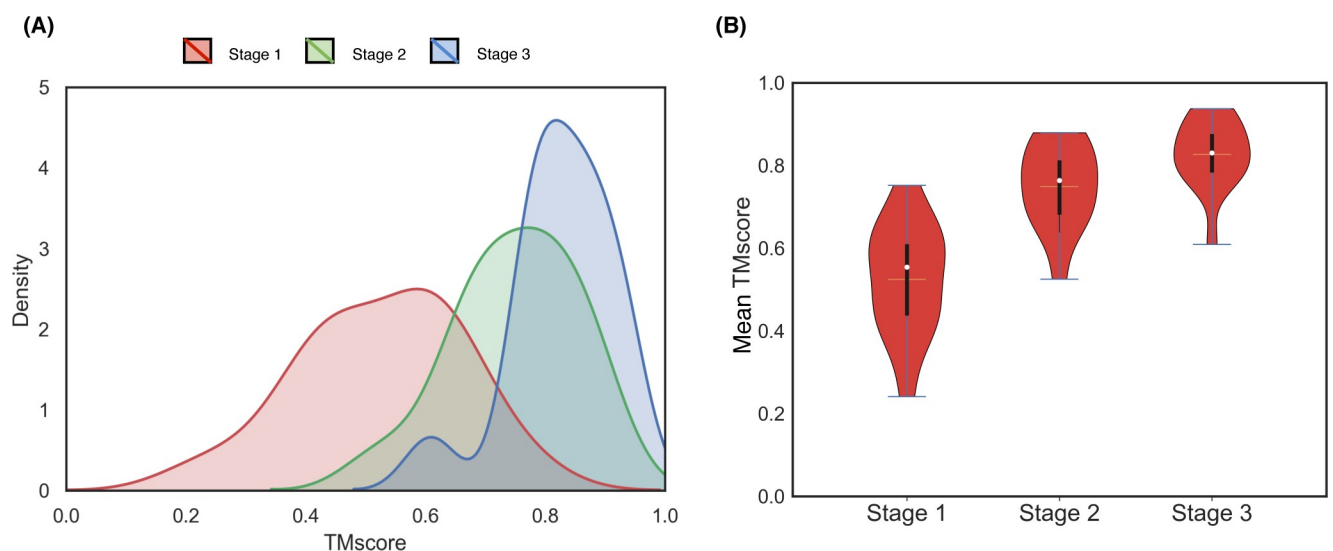


**Fig 8. Stages TM-score distributions of the reconstructed models on 15 proteins from the EVfold set.** Stage-by-stage (A) density plots and (B) violin plots are shown with the means indicated using the unfilled circles, the medians indicated using the horizontal yellow lines, and the interquartile ranges indicated using the vertical black strips.

<https://doi.org/10.1371/journal.pcbi.1008753.g008>





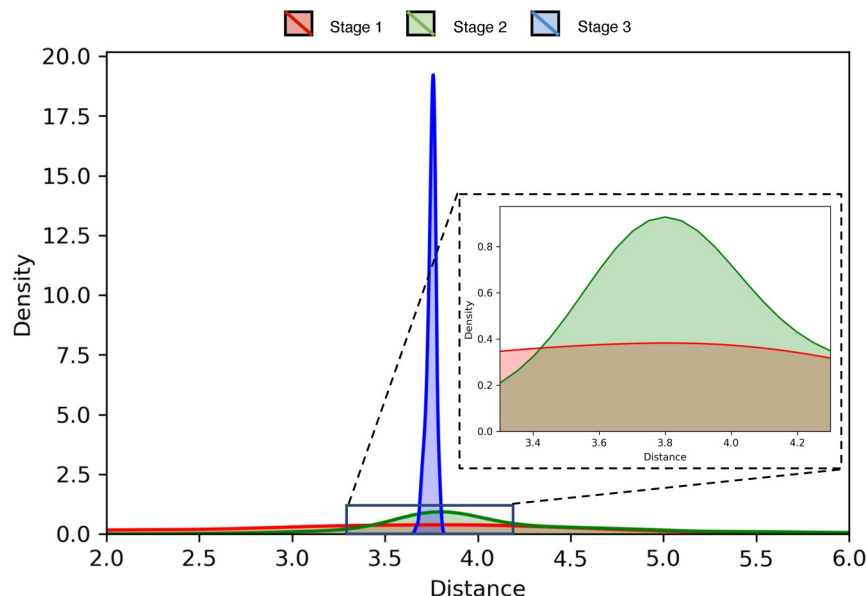


**Fig 10. Stagewise distributions of the pseudo-covalent bond lengths for the protein target (PDB ID 5p21 and chain A).** The inset magnifies the stage 1 and stage 2 distributions around the ideal value of 3.8 Å.

<https://doi.org/10.1371/journal.pcbi.1008753.g010>

in DConStruct cooperatively improve the global fold-level accuracy and local secondary structural topology, while progressively reducing the inconsistencies in pseudo-covalent geometry, thus gradually making the structure consistent with a physically realistic protein conformation.

### Why does DConStruct attain better accuracy at higher-thresholded contact maps?

An interesting finding is that DConStruct attains better folding performance for the interaction maps at higher contact thresholds such as 10 and 12 Å. To unravel the underlying cause of such trend, we perform stage-by-stage 3D reconstruction on the same EVfold dataset comprising of 15 proteins by varying contact thresholds from 8 to 12 Å in a step size of 2 Å with true secondary structures, and study the gain in folding performance caused by the introduction of stage 2 ( $\Delta_2$ ) and stage 3 ( $\Delta_3$ ).

As reported in [Table 7](#) by using true  $C_\beta$ - $C_\beta$  contacts, the mean  $\Delta_2$  (gain by stage 2) significantly increases with the increase in contact threshold in that  $\Delta_2$  gets more than doubled from 0.22 at 8 Å threshold to 0.46 at 12 Å threshold. The mean  $\Delta_3$  (gain by stage 3), on the other hand, remains relatively constant at around 0.07. This implies that stage 2 is the main driver of the improved folding accuracy for higher-thresholded contact maps ([S10 Table](#)). The results remain very similar when we repeat the experiment with the true  $C_\alpha$ - $C_\alpha$  contacts ([S11 Table](#)). To further understand whether an increase in distance threshold has any effect on the secondary structure topology, we study stage-wise  $Q_H$  and  $Q_E$  at varying contact thresholds from 8 to 12 Å using both  $C_\beta$ - $C_\beta$  ([S12 Table](#)) and  $C_\alpha$ - $C_\alpha$  contacts ([S13 Table](#)). This time, stage 3 shows noticeable gain in beta strand topology with ~10–15% increase in  $Q_E$  as contact threshold increases from 8 to 12 Å, while the gain in  $Q_H$  achieved by stage 2 remains almost constant at higher-thresholded contact maps. In summary, these results further emphasize the cooperative aspect of the hierarchical modeling approach used in DConStruct, and indicate that the

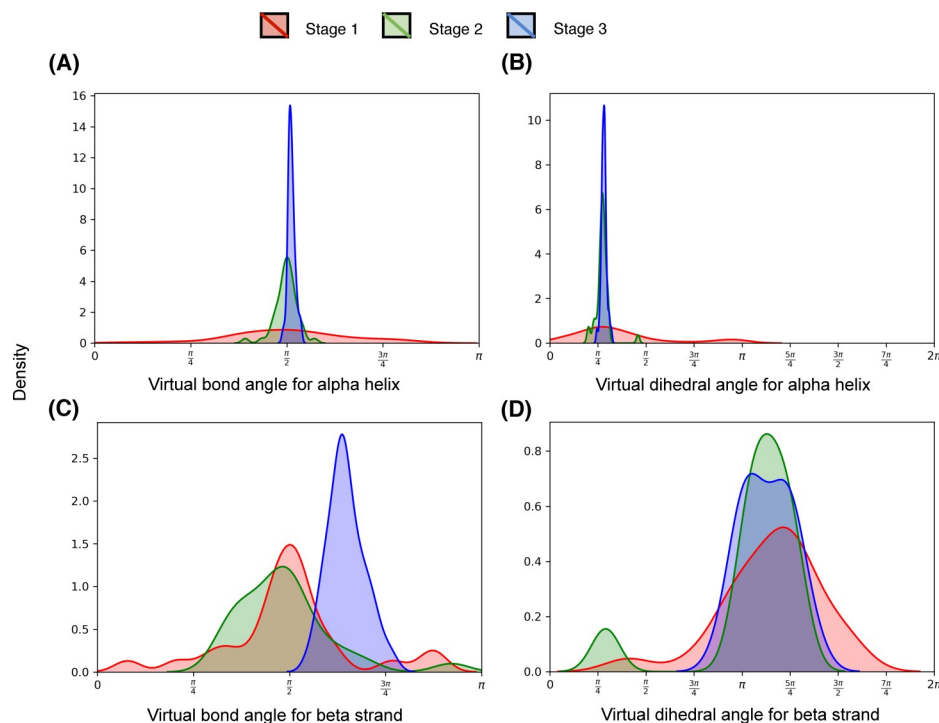


**Fig 11. Stagewise distributions of the virtual bond and dihedral angles for residues in (A-B) alpha helices and (C-D) beta strands for the protein target (PDB ID 5p21 and chain A).**

<https://doi.org/10.1371/journal.pcbi.1008753.g011>

improved folding accuracy at higher-thresholded contact maps is the result of the combined improvement in the fold-level accuracy by stage 2 and enhancement in long-range hydrogen bonds formation for stabilizing the beta sheet geometry by stage 3.

**Table 7. TM-score gain  $\Delta_2$  (TM-score of stage 2 – TM-score of stage 1) and  $\Delta_3$  (TM-score of stage 3 – TM-score of stage 2) after performing stage-by-stage 3D reconstruction for 15 protein targets in EVfold dataset using true  $C_\beta$ - $C_\beta$  contact maps at 8, 10, and 12Å thresholds and true secondary structures.**

Target	8Å		10Å		12Å	
	$\Delta_2$	$\Delta_3$	$\Delta_2$	$\Delta_3$	$\Delta_2$	$\Delta_3$
1bkrA	0.12	0.04	0.27	0.06	0.46	0.06
1e6kA	0.19	0.08	0.33	0.07	0.46	0.05
1f21A	0.17	0.06	0.33	0.06	0.46	0.03
1g2eA	0.24	0.10	0.37	0.07	0.48	0.09
1hzzA	0.12	0.04	0.31	0.04	0.51	0.02
1oddA	0.08	0.10	0.32	0.12	0.39	0.14
1r9hA	0.30	0.08	0.38	0.06	0.52	0.05
1rqmA	0.21	0.04	0.35	0.02	0.48	0.03
1wvnA	0.26	0.07	0.35	0.05	0.42	0.05
2hdaA	0.28	0.08	0.39	0.12	0.38	0.13
2it6A	0.27	0.08	0.39	0.09	0.51	0.05
2o72A	0.33	0.10	0.42	0.09	0.50	0.10
3tgiE	0.24	0.06	0.37	0.04	0.48	0.03
5p21A	0.27	0.05	0.34	0.04	0.48	0.05
5ptiA	0.20	0.15	0.33	0.12	0.38	0.12
Mean	0.22	0.08	0.35	0.07	0.46	0.07

<https://doi.org/10.1371/journal.pcbi.1008753.t007>

## Discussion

This article has presented a new hybridized distance- and contact-based hierarchical structure modeling method DConStruct that can greatly improve *ab initio* protein folding. In contrast to the existing folding approaches, our method neither depends on the CNS experimental structure determination protocol nor performs time-consuming fragment-based conformational sampling, but rather employs 3-stage hierarchical structure modeling driven purely by the geometric restraints induced by inter-residue interaction maps and secondary structures. Our new predictive modeling method DConStruct is unique in that it can hierarchically estimate the correct overall fold of a target protein in coarse-grained mode to progressively optimize the local and non-local interactions while enhancing secondary structure topology in a self-correcting manner. Rigorous experimental validation reveals that DConStruct not only attains much better contact-driven reconstruction performance than currently popular CNS-based approaches, but also scales at a much higher degree of folding accuracy than CNS with the increase in contact thresholds. DConStruct is also versatile in that it can exploit the information encoded in the interaction maps at multiple granularities ranging from binary contact maps to distance-based hybrid maps at tri-level thresholding, which results in better *ab initio* folding performance for CASP12 and CASP13 FM targets compared to several popular CNS- and fragment-based approaches as well as energy-minimization protocols. Even without using fine-grained distance maps or fragment assembly, *ab initio* folding using DConStruct can yield the correct fold for more CASP FM targets than state-of-the-art approaches. Further, our experimental results show that DConStruct leads to better folding accuracy for membrane proteins compared to a CNS-based approach. We expect that our new structure modeling method can enhance the accuracy of distance- or contact-driven folding of many more non-homologous proteins that lack experimental structures, thereby facilitating structure-based studies for additional protein families, leading to new biological insights.

Our method outperforms CNS due to a couple of reasons. First, CNS combines the restraints derived from the interaction maps with an in-built biophysical force field having parameters fine-tuned for experimental data, while our method is free from the influence of such force fields. Second, CNS adopts an all-atom representation throughout the folding simulation, while our new method DConStruct follows a hierarchic approach by first estimating the correct overall fold in coarse-grained mode and then progressively optimizing the local and non-local interactions in atomistic detail. As such, the adaptation of coarse-grained representation in DConStruct during the early stages of folding significantly reduces the conformational space, accelerating the estimation of the overall fold driven purely by the inter-residue interactions defined between the  $C_{\alpha}$ - $C_{\alpha}$  or  $C_{\beta}$ - $C_{\beta}$  atom pairs. Finally, the introduction of additional folding stages in DConStruct cooperatively improves the overall fold and facilitates hydrogen bonds formation for stabilizing the secondary structure topologies, ultimately resulting in improved folding performance compared to CNS.

The hierarchical structure modeling paradigm employed in DConStruct attains better folding accuracy than CNS-based CONFOLD protocol for higher-thresholded contact maps at 10 and 12Å, beyond the standard contact threshold of 8Å currently used by the community. Experimental results show that this behavior is attributed to the cooperative nature of the 3-stage hierarchical modeling approach adopted in DConStruct, with stage 2 further improving the fold-level accuracy with the increase in contact threshold than the initial fold estimated by the coarse-grained modeling from stage 1, and stage 3 better enhancing long-range hydrogen bonds formation for stabilizing the beta sheet geometry at higher-thresholded contact maps. Moreover, feeding hybrid interaction maps at tri-level thresholding that combines contact maps at 8, 10, and 12Å thresholds further improves the performance of DConStruct,

opening the unique possibility of utilizing hybridized distance and contact maps for predictive protein modeling. Indeed, our hybridized distance- and contact-based hierarchical folding method DConStruct delivers better performance in *ab initio* folding of CASP free modeling targets compared to CNS-based CONFOLD2 and DMPfold protocols as well as ROSETTA-based fragment assembly pipeline PconsFold and recent fragment-based CGLfold method. DConStruct convincingly outperforms the DMPfold protocol, which uses much finer-grained distance maps along with additional predicted structural features such as torsion angles and hydrogen bonds, whereas our method utilizes only hybrid interaction maps at tri-level thresholding derived from the DMPfold-predicted initial distance histograms. Additionally, DConStruct attains better performance than distance-based trRosetta protocol. The better predictive modeling performance of DConStruct also translates to superior *ab initio* folding of membrane proteins compared to the state of the art. In summary, the advantage of DConStruct in *de novo* protein modeling over the others is significant.

We may further improve the folding accuracy of our new method by extending the hierarchical structure modeling by allowing finer-grained distance intervals, which contain more information than what we are using now. For example, we may directly feed all the distance bins from DMPfold or trRosetta with their likelihood values to DConStruct during predictive modeling. The recently concluded CASP14 experiment has expanded the contact prediction category by introducing a new RR format that includes fine-grained inter-residue distance histogram prediction. The newly introduced RR format includes 10 distance intervals:  $<4\text{\AA}$ , 4–6  $\text{\AA}$ , 6–8  $\text{\AA}$ , 8–10  $\text{\AA}$ , 10–12  $\text{\AA}$ , 12–14  $\text{\AA}$ , 14–16  $\text{\AA}$ , 16–18  $\text{\AA}$ , 18–20  $\text{\AA}$ , and  $>20\text{\AA}$ . Due to the inherent flexibility of DConStruct that can utilize any distance histogram predicted by any method, the fine-grained predicted distance information having 10 intervals can be directly fed into DConStruct for predictive modeling instead of the hybrid interaction maps at tri-level thresholding. Combining various complementary approaches for predicting fine-grained distance maps can also be explored. Needless to say, accurate estimation of finer-grained distance maps is a very challenging problem, which may suffer from high false-positive rates and thus prone to be noisy. Empowering our method to be robust and noise-tolerant while utilizing finer-grained distance intervals shall result in much better 3D models. To utilize the input distance information more effectively, we may employ an efficient geometric build-up algorithm with least-square approximation [44], which has been shown to be noise-tolerant. With the help of the geometric build-up algorithm, the missing entries in inter-residue proximity maps can be potentially approximated more accurately, which might further improve the generation of the proximity map from a sparse set of distances, possibly resulting in more accurate coarse-grained models. We may also improve the hierarchical structure modeling by performing enhanced sampling targeted at the regions not restrained by input interaction maps. This may improve the quality of the flexible loops or terminal regions, which may not be proximal to the core regions, ultimately enhancing the overall folding accuracy. In this regard, the choice of an optimal representation that can strike a balance between the conformational space and modeling granularity can be a related potential area of improvement. DConStruct currently imposes  $C_\beta$  constraints only at stage 3 whereas stage 1 and stage 2 operates on a  $C_\alpha$ -only mode. We could explore the possibility of adopting a unified representation having both  $C_\alpha$  and  $C_\beta$  atoms during the early modeling stages for potentially improved folding performance, even though the addition of the  $C_\beta$  atoms leads to increased conformational space that may undermine some of the advantages of the coarse-grained representation adopted by DConStruct. Furthermore, we may leverage additional information from the existing literature obtained from rigorous statistical analyses of residue-level and secondary structure-specific distances and angles [43]. For example, we may augment additional knowledge-based constraints derived from the correlation of residue-level and secondary structure-specific pseudo-covalent



bond lengths and virtual bond and dihedral angles. In addition to secondary structure, contact and/or distance information, our method can also be extended to use other structural features such as inter-residue orientation, solvent accessibility, and disulfide bridges, which contain complementary information about protein conformation, and thus, shall benefit predictive structure modeling. The results of the recently concluded CASP14 experiment indicate dramatic progress in protein structure prediction by the emergence of the new AlphaFold2 method attaining an average TM-score of 0.84 for the CASP14 free modeling targets. AlphaFold2 represents a significant improvement over the AlphaFold method employed in A7D during CASP13. It might be interesting to explore the possibility of coupling our folding protocol with the predicted structural information utilized by AlphaFold2 and compare the folding performance as the details of the AlphaFold2 method becomes available.

## Methods

### Hierarchical structure modeling employed in DConStruct

**From interaction map and secondary structure to proximity map.** Our folding protocol starts by estimating the proximity map from a given interaction map and secondary structure using knowledge-based and graph-theoretic approach. Simply speaking, a proximity map is an approximation of the inter-residue distance matrix. Using a coarse-grained string of beads representation, in which each bead corresponds to the  $C_\alpha$  atom of an amino acid residue, we first estimate the proximity between the residue pairs close in sequence from prior knowledge of protein backbone geometry derived from the pseudo-covalent bonds formed between the  $C_\alpha$  atoms and the secondary structure-specific local structural preferences [21,36], thus generating a sparse proximity map. For sequentially distant residue pairs, we apply a graph-theoretic approach to fill the missing entries in the proximity map. We treat the input interaction map as an adjacency matrix representing a graph  $G = (V, E)$ , where  $V = \{v_1, v_2, \dots\}$  is the set of nodes, representing a residue's  $C_\alpha$  (or  $C_\beta$ ) atom, and  $E = \{e_{ij}\}$  is the set of edges, where  $e_{ij}$  represents the interaction (e.g., residue-residue contact) between  $v_i$  and  $v_j$ . Thus, the graph  $G$  encapsulates the mathematical relation of inter-residue spatial proximity in 3D space. A graph distance function [37,45], defined as the shortest path length among all paths for any given residue pair, can be applied to the graph that shall be measured for the entire set of  $V$ . The path length can be calculated by summing the total number of edges connecting any pair of residues ( $v_i, v_j$ ) under consideration. This function approximates the spatial distances and can generate an initial estimate of the proximity map. Here we use Floyd-Warshall all pair shortest path algorithm [46] to compute the path length. We further refine the initial estimate of the proximity map by idealized secondary structure element (SSE) modeling. SSEs are identified from the given secondary structure and are independently modeled by setting the sequence of pseudo angles and pseudo dihedral angles spanning each SSE to their ideal values [21,47]. The SSEs, modeled in angular space, are subsequently converted into Cartesian space assuming the distance between two consecutive residues is constant (3.8Å) to extract the intra-SSE-all-residue-pairs distances for refining the initial proximity map. The rationale for this step is to enhance the physical realism of the proximity map for the intra-SSE segments.

**From proximity map to coarse-grained 3D models.** We turn the proximity map into a 3D model using an efficient graph realization technique. The basic idea is to treat the graph distance-based proximity information between  $C_\alpha$  atoms for each residue pair to calculate the corresponding coordinates for all residues by applying the graph-based method, multidimensional scaling (MDS) [22–24], for generating coarse-grained 3D models. MDS starts with dissimilarity matrices that are derived from points in a multidimensional space, and it finds the positioning of the points in a low-dimensional space, where the distances between points

resemble the original dissimilarities. Here, we use the proximity map between the  $C_\alpha$  atoms of each residue pair as dissimilarity matrix and then calculate the coordinates of the  $C_\alpha$  atom for all residue. If there are  $n$  points (each representing the  $C_\alpha$  atom of a residue)  $X_k \in \mathbb{R}^3$ ,  $k = 1, \dots, n$  in 3D. Here we use classical metric MDS (CMDS) [48], which is the first and simplest MDS algorithm. For a perfect dissimilarity (distance) matrix without any error in the Euclidean space, CMDS will exactly reconstruct the configuration of points (or its mirror configuration) with a computational complexity of  $O(n^3)$ . But, when there are errors in the dissimilarity matrix, CMDS minimizes the sum of least squared errors between the estimated and the observed distances in the output model for all pairs of points. In practice, the technique gracefully tolerates errors due to the overdetermined nature of the solutions. This is important in our case, as our graph-based proximity map is an approximation of the true Euclidean distance matrix that can be noisy and physically unrealistic, particularly for sequentially distant residue pairs. We iteratively apply this technique to produce an initial pool of 20 coarse-grained 3D models by enumerating over 20 different random seeds in order to achieve conformational diversity in the resulting model pool.

**Improving coarse-grained models through iterative self-correction.** We apply iterative self-correction via local perturbation to further optimize the coarse-grained models. Specifically, we identify the residues having inconsistent spatial positioning with respect to the rest of the structure and employ coordinate refinement heuristics [49] to correct its coordinate without introducing new error in the coordinate set. For the residue-pairs having their Euclidean distances close to the distance threshold of the input interaction map, we apply corrective coordinate perturbation to maximally reproduce contacts and non-contacts. We also perform local perturbation for intra-SSE-segments by coordinate adjustments without affecting other correctly positioned residues outside of SSE. Furthermore, we enforce idealized pseudo-covalent bond lengths constraints formed between consecutive  $C_\alpha$  atoms ( $3.8\text{\AA}$ ), and steric clash constraints (defined as two  $C_\alpha$  atoms that are closer than  $3.5\text{\AA}$  from each other). Specifically, for the consecutive  $C_\alpha$  atoms, we calculate the pseudo-covalent bond lengths formed in the coarse-grained models and determine the deviations from the ideal value of  $3.8\text{\AA}$ , which we then use to correct the coordinate of each  $C_\alpha$  atom by moving it towards or to the opposite direction of its adjacent  $C_\alpha$  atom in the Cartesian space. Finally, we employ Limited-memory Broyden-Fletcher-Goldfarb-Shannon (L-BFGS) [25] algorithm for minimizing a harmonic function of the observed and expected distance values of  $C_\alpha$  quadruplets ( $i-1, i+1, i+2, i+3$ ); with distances between the  $(i-1)$ th residue and the  $(i+1)$ th, the  $(i+2)$ th, and the  $(i+3)$ th residues, respectively. The expected values specific to helices and strands are adopted from existing literature [21] to refine the local secondary structure topology. The entire self-correction process described above is iteratively applied to generate a pool of 20 optimized 3D models.

**Contact violation-based model selection and geometric chirality checking.** For the selection of one representative structure from the optimized model pool, we use a contact violation-based score function that combines contact or non-contact satisfaction of a model as:  $F = \sum \text{contact-error} + \sum \text{non-contact-error} + n'$ , where contact- and non-contact-errors are calculated using a squared error function, defined as  $(d_{ij} - \text{threshold})^2$  for residue-pair  $(i, j)$  with distance  $d_{ij}$  that violates input contacts (or non-contacts), and  $n'$  is the number of residue pairs inconsistent with the input interaction map. We rank the pool of optimized models using this score function to select the highest ranked model as the representative.

One remaining issue in our selected model is that it can be a mirror image of the biologically relevant 3D conformation that has the correct chirality or handedness at the local level. This is a typical issue faced during the reconstruction of 3D structure from a 2D representation since any distance function is invariant to the isometric transformations in 3D: translation,

rotation and symmetry. As such, it is not obvious which of the two structures related by mirror symmetry represents a biologically relevant structure. Nonetheless, secondary structure can be used to identify the correct chirality of a 3D conformation since the observed chirality is mostly right-handed for  $\alpha$ -helices and left-handed  $\beta$ -sheets [26]. We define a geometric cost function for identifying the correct chirality as the sum over tetrapeptides in  $\alpha$ -helices and  $\beta$ -sheets by utilizing the secondary structure-specific normalized triple scalar product values adopted from existing literature [26]. From among the two mirror images of the selected model, we select the structure with lowest cost as the correct chirality.

**Atomic-level model building and iterative self-correction.** We use MODELLER [27] to generate atomic-level model and perform restraint satisfaction using the secondary structure and interaction map-derived geometric restraints to generate optimized atomic-level model, and subsequently employ restraint satisfaction iteratively using unsatisfied interactions, non-interactions, and secondary structure restraints for self-correction along with model combination to generate the final folded conformation.

## Test datasets and programs to compare

For the 3D reconstruction from the true contact-based interaction map and true secondary structure, we use 150 soluble proteins from FRAGFOLD [28] dataset with sequence length ranging from 50 to 266 residues. We extract the true contact maps from the experimental structures having a sequence separation of at least 6 residues by varying the contact thresholds from 8 to 12 Å in a step size of 0.5 Å. We use DSSP [38] program to compute the true secondary structures from the experimental structures. We compare DConStruct with two widely used reconstruction methods, FT-COMAR [36] and CONFOLD [17], using the same input. FT-COMAR is a fast and purely distance geometry-based heuristic method that reconstructs the  $C_\alpha$  trace purely from a given  $C_\alpha$ - $C_\alpha$  contact matrix and does not accept secondary structure. On the other hand, CNS-based CONFOLD reconstructs protein 3D structure using a contact map and a secondary structure via a two-stage process. For CONFOLD-based reconstruction, we set the parameters of CONFOLD as ‘-stage2 3’ (model generation at stage 2 using sheet-detection only for true contacts), ‘-rep 0.8’ (used for true contact), ‘-rrtype cb’ (for  $C_\beta$ - $C_\beta$  contacts) or ‘-rrtype ca’ (for  $C_\alpha$ - $C_\alpha$  contacts). Furthermore, we extract the true distance-based hybrid interaction maps (both  $C_\alpha$ - $C_\alpha$  and  $C_\beta$ - $C_\beta$ ) from the experimental structures and use them together with their true secondary structures for 3D reconstruction using DConStruct.

For *ab initio* folding, 40 free modeling (FM) domains from CASP12 and CASP13 with publicly available experimental structures are used with target lengths ranging from 67 to 356 residues. The performance of DConStruct is compared with DMPfold [8], CONFOLD2 [18], ROSETTA [13] and CGLFold [15], GDFuzz3D [37], trRosetta [33] and several top predictors participated in CASP12 and CASP13. DMPfold is a deep learning-based CNS-dependent *ab initio* folding method. CONFOLD2 is a modified version of CONFOLD based on CNS-based distance geometry algorithm. For *ab initio* folding using CONFOLD2, RaptorX predicted top 2L contacts, obtained by submitting jobs to its web server, are used according to the published paper [4], together with the secondary structures predicted using SPIDER3 [34]. For ROSETTA, we adopt a similar process as in PconsFold [14] protocol with the only exception of using RaptorX contacts instead of PconsC [50]. We obtain fragments (3-mers and 9-mers) from the ROSETTA server [51] to generate a pool of 2,000 models with a maximum duration of 15 calendar days. The lowest ROSETTA energy models are subsequently selected as the prediction. CGLFold [15] is a recent fragment-based method that combines global exploration and loop perturbation using the predicted contact maps from ResTriplet [52]. The TM-scores for CGLFold 29 FM targets are collected from its published paper. GDFuzz3D [37] uses a

multi-step modeling that involves a combination of coarse-grained and all-atom modeling. For GDFuzz3D, we submit jobs to its web server, which is limited to protein size of less than 400 residues. We, therefore, collect GDFuzz3D predicted models for 28 CASP FM targets having length less than 400 residues by feeding the RaptorX predicted contacts to its web server. trRosetta [33] is a state-of-the-art deep learning-based transform-restrained energy-minimization protocol. We run trRosetta-based modeling locally with the parameter setting ('-no-orient') that uses the fine-grained distance information predicted from trRosetta but no orientation information for a head-to-head performance comparison with DConStruct. To generate distance-based hybrid interaction maps for DConStruct, we use the DMPfold distance predictor. We feed the multiple sequence alignments (MSAs) [35] to DMPfold and obtain the predicted initial distance histograms (rawdispred.current files) containing 20 distance bins with their associated likelihoods (we do not run any further DMPfold iterations involving CNS-based modeling). The predicted histograms are then converted to hybrid interaction maps with tri-level thresholding with variable upper bounds of 8, 10, and 12 Å by summing up the likelihoods for distance bins below the three distance thresholds of 8, 10, and 12 Å. We select the top 8L  $C_{\beta}$ - $C_{\beta}$  high confidence interacting residue pairs having likelihoods  $> 0.85$  since using the top 8L  $C_{\beta}$ - $C_{\beta}$  contacts delivers the best performance in an independent benchmarking on the EVfold dataset (S14 Table) when experimented with top 2L, 4L, 8L, and 16L  $C_{\beta}$ - $C_{\beta}$  contacts. A similar strategy is followed to derive hybrid interaction maps from trRosetta-predicted distance maps. The hybrid interaction maps coupled with the SPIDER3 predicted secondary structures are then fed to DConStruct for *ab initio* folding.

We also evaluate *ab initio* folding of membrane proteins using 510 non-redundant membrane proteins used in [31] with length ranging from 50 to 646 residues. We generate the distance-based hybrid interaction maps using DMPfold as mentioned above and predict their 3D structures using DConStruct to compare our models with that of Xu's deep transfer learning (DTL) and CNS-based *ab initio* folding method [31].

To evaluate the implications of the 3-stage hierarchical structure modeling approach adopted in DConStruct, we use 15 proteins from the EVfold [16] dataset ranging from 48 to 248 residues in length. We use true contact interactions with a sequence separation of at least 6 residues and true secondary structures to perform stage-by-stage 3D reconstruction and analysis after using the PULCHRA program [53] to generate all-atom models from the coarse-grained models produced in the intermediate stages.

## Evaluation metrics

We use TM-score [39] to evaluate the folding accuracy. TM-score compares the predicted models with the experimental structure to determine their structural similarity. TM-score has the value in (0, 1], with higher value indicating better folding accuracy. Meanwhile, TM-score  $> 0.5$  represents correctly folded models [40]. We measure the correctness of secondary structure topology using the percentage of correctly recovered secondary structure residues for helices ( $Q_H$ ) and beta strands ( $Q_E$ ).

## Supporting information

**S1 Table. Target-by-target reconstruction performance on 150 soluble proteins for true  $C_{\alpha}$ - $C_{\alpha}$  contact maps at various thresholds.**  
(DOCX)

**S2 Table. Target-by-target reconstruction performance on 150 soluble proteins for true  $C_\beta$ - $C_\beta$  contact maps at various thresholds.**  
(DOCX)

**S3 Table. Target-by-target reconstruction performance on 150 soluble proteins for true  $C_\alpha$ - $C_\alpha$  hybrid interaction maps at tri-level thresholding.**  
(DOCX)

**S4 Table. Target-by-target reconstruction performance on 150 soluble proteins for true  $C_\beta$ - $C_\beta$  hybrid interaction maps at tri-level thresholding.**  
(DOCX)

**S5 Table. Target-by-target *ab initio* folding performance on 40 CASP FM targets.**  
(DOCX)

**S6 Table. Target-by-target *ab initio* folding performance on a subset of 29 CASP FM targets relevant to CGLFold.**  
(DOCX)

**S7 Table. Target-by-target *ab initio* folding performance on a subset of 28 CASP FM targets relevant to GDFuzz3D.**  
(DOCX)

**S8 Table. Target-by-target *ab initio* folding performance of top CASP human and server predictors, DConStruct with trRosetta distance maps, customized DMPfold, and trRosetta on 40 CASP FM targets.**  
(DOCX)

**S9 Table. Target-by-target *ab initio* folding performance on 510 membrane proteins.**  
(DOCX)

**S10 Table. Target-by-target stagewise reconstruction performance on EVfold dataset for true  $C_\beta$ - $C_\beta$  contact maps at 8, 10, and 12Å thresholds.**  
(DOCX)

**S11 Table. Target-by-target stagewise reconstruction performance on EVfold dataset for true  $C_\alpha$ - $C_\alpha$  contact maps at 8, 10, and 12Å thresholds.**  
(DOCX)

**S12 Table. Target-by-target stagewise recovery of secondary structure topology on EVfold dataset for true  $C_\beta$ - $C_\beta$  contact maps at 8, 10, and 12Å thresholds.**  
(DOCX)

**S13 Table. Target-by-target stagewise recovery of secondary structure topology on EVfold dataset for true  $C_\alpha$ - $C_\alpha$  contact maps at 8, 10, and 12Å thresholds.**  
(DOCX)

**S14 Table. *Ab initio* folding performance of DConStruct on EVfold dataset using top hybrid interaction maps with tri-level thresholding at increasing xL values (x = 2, 4, 8, 16).**  
(DOCX)

## Acknowledgments

This work was made possible in part by a grant of high performance computing resources and technical support from the Alabama Supercomputer Authority and the Extreme Science and Engineering Discovery Environment (XSEDE).



## Author Contributions

**Conceptualization:** Debswapna Bhattacharya.

**Data curation:** Rahmatullah Roche.

**Formal analysis:** Rahmatullah Roche, Debswapna Bhattacharya.

**Funding acquisition:** Debswapna Bhattacharya.

**Investigation:** Rahmatullah Roche, Debswapna Bhattacharya.

**Methodology:** Debswapna Bhattacharya.

**Project administration:** Debswapna Bhattacharya.

**Resources:** Debswapna Bhattacharya.

**Software:** Rahmatullah Roche, Sutanu Bhattacharya, Debswapna Bhattacharya.

**Supervision:** Debswapna Bhattacharya.

**Validation:** Rahmatullah Roche, Sutanu Bhattacharya, Debswapna Bhattacharya.

**Visualization:** Rahmatullah Roche, Debswapna Bhattacharya.

**Writing – original draft:** Rahmatullah Roche, Debswapna Bhattacharya.

**Writing – review & editing:** Debswapna Bhattacharya.

## References

1. Dill KA, MacCallum JL. The Protein-Folding Problem, 50 Years On. *Science*. 2012; 338: 1042–1046. <https://doi.org/10.1126/science.1219021> PMID: 23180855
2. de Juan D, Pazos F, Valencia A. Emerging methods in protein co-evolution. *Nat Rev Genet*. 2013; 14: 249–261. <https://doi.org/10.1038/nrg3414> PMID: 23458856
3. Marks DS, Hopf TA, Sander C. Protein structure prediction from sequence variation. *Nature Biotechnology*. 2012; 30: 1072–1080. <https://doi.org/10.1038/nbt.2419> PMID: 23138306
4. Wang S, Sun S, Li Z, Zhang R, Xu J. Accurate De Novo Prediction of Protein Contact Map by Ultra-Deep Learning Model. *PLOS Computational Biology*. 2017; 13: e1005324. <https://doi.org/10.1371/journal.pcbi.1005324> PMID: 28056090
5. Kandathil SM, Greener JG, Jones DT. Prediction of interresidue contacts with DeepMetaPSICOV in CASP13. *Proteins: Structure, Function, and Bioinformatics*. 2019; 87: 1092–1099. <https://doi.org/10.1002/prot.25779> PMID: 31298436
6. Li Y, Hu J, Zhang C, Yu D-J, Zhang Y. ResPRE: high-accuracy protein contact prediction by coupling precision matrix with deep residual neural networks. *Bioinformatics*. 2019; 35: 4647–4655. <https://doi.org/10.1093/bioinformatics/btz291> PMID: 31070716
7. Senior AW, Evans R, Jumper J, Kirkpatrick J, Sifre L, Green T, et al. Protein structure prediction using multiple deep neural networks in the 13th Critical Assessment of Protein Structure Prediction (CASP13). *Proteins: Structure, Function, and Bioinformatics*. 2019; 87: 1141–1148. <https://doi.org/10.1002/prot.25834> PMID: 31602685
8. Greener JG, Kandathil SM, Jones DT. Deep learning extends de novo protein modelling coverage of genomes using iteratively predicted structural constraints. *Nat Commun*. 2019; 10: 1–13. <https://doi.org/10.1038/s41467-018-07882-8> PMID: 30602773
9. Xu J. Distance-based protein folding powered by deep learning. *PNAS*. 2019; 116: 16856–16865. <https://doi.org/10.1073/pnas.1821309116> PMID: 31399549
10. Buchan DWA, Jones DT. Improved protein contact predictions with the MetaPSICOV2 server in CASP12. *Proteins: Structure, Function, and Bioinformatics*. 2018; 86: 78–83. <https://doi.org/10.1002/prot.25379> PMID: 28901583
11. Abriata LA, Tamò GE, Peraro MD. A further leap of improvement in tertiary structure prediction in CASP13 prompts new routes for future assessments. *Proteins: Structure, Function, and Bioinformatics*. 2019; 87: 1100–1112. <https://doi.org/10.1002/prot.25787> PMID: 31344267

12. Kandathil SM, Greener JG, Jones DT. Recent developments in deep learning applied to protein structure prediction. *Proteins: Structure, Function, and Bioinformatics*. 2019; 87: 1179–1189. <https://doi.org/10.1002/prot.25824> PMID: 31589782
13. Leaver-Fay A, Tyka M, Lewis SM, Lange OF, Thompson J, Jacak R, et al. ROSETTA3: an object-oriented software suite for the simulation and design of macromolecules. *Meth Enzymol*. 2011; 487: 545–574. <https://doi.org/10.1016/B978-0-12-381270-4.00019-6> PMID: 21187238
14. Michel M, Hayat S, Skwark MJ, Sander C, Marks DS, Elofsson A. PconsFold: improved contact predictions improve protein models. *Bioinformatics*. 2014; 30: i482–i488. <https://doi.org/10.1093/bioinformatics/btu458> PMID: 25161237
15. Liu J, Zhou X-G, Zhang Y, Zhang G-J. CGLFold: a contact-assisted de novo protein structure prediction using global exploration and loop perturbation sampling algorithm. *Bioinformatics*. 2020; 36: 2443–2450. <https://doi.org/10.1093/bioinformatics/btz943> PMID: 31860059
16. Marks DS, Colwell LJ, Sheridan R, Hopf TA, Pagnani A, Zecchina R, et al. Protein 3D structure computed from evolutionary sequence variation. *PLoS ONE*. 2011; 6: e28766. <https://doi.org/10.1371/journal.pone.0028766> PMID: 22163331
17. Adhikari B, Bhattacharya D, Cao R, Cheng J. CONFOLD: Residue-residue contact-guided ab initio protein folding. *Proteins: Structure, Function, and Bioinformatics*. 2015; 83: 1436–1449. <https://doi.org/10.1002/prot.24829> PMID: 25974172
18. Adhikari B, Cheng J. CONFOLD2: improved contact-driven ab initio protein structure modeling. *BMC Bioinformatics*. 2018; 19: 22. <https://doi.org/10.1186/s12859-018-2032-6> PMID: 29370750
19. Wang S, Li W, Zhang R, Liu S, Xu J. CoinFold: a web server for protein contact prediction and contact-assisted protein folding. *Nucleic Acids Res*. 2016; 44: W361–W366. <https://doi.org/10.1093/nar/gkw307> PMID: 27112569
20. Brunger AT. Version 1.2 of the Crystallography and NMR system. *Nature Protocols*. 2007; 2: 2728–2733. <https://doi.org/10.1038/nprot.2007.406> PMID: 18007608
21. Labesse G, Colloc'h N, Pothier J, Mornon J-P. P-SEA: a new efficient assignment of secondary structure from Cα trace of proteins. *Bioinformatics*. 1997; 13: 291–295. <https://doi.org/10.1093/bioinformatics/13.3.291> PMID: 9183534
22. Borg I, Groenen PJF. *Modern Multidimensional Scaling: Theory and Applications*. 2nd ed. New York: Springer-Verlag; 2005.
23. Kruskal JB. Nonmetric multidimensional scaling: A numerical method. *Psychometrika*. 1964; 29: 115–129. <https://doi.org/10.1007/BF02289694>
24. Kruskal JB. Multidimensional scaling by optimizing goodness of fit to a nonmetric hypothesis. *Psychometrika*. 1964; 29: 1–27. <https://doi.org/10.1007/BF02289565>
25. Liu DC, Nocedal J. On the limited memory BFGS method for large scale optimization. *Mathematical Programming*. 1989; 45: 503–528. <https://doi.org/10.1007/BF01589116>
26. Lund O, Hansen J, Brunak S, Bohr J. Relationship between protein structure and geometrical constraints. *Protein Sci*. 1996; 5: 2217–2225. <https://doi.org/10.1002/pro.5560051108> PMID: 8931140
27. Sali A, Blundell TL. Comparative protein modelling by satisfaction of spatial restraints. *J Mol Biol*. 1993; 234: 779–815. <https://doi.org/10.1006/jmbi.1993.1626> PMID: 8254673
28. Jones DT. Predicting novel protein folds by using FRAGFOLD. *Proteins: Structure, Function, and Bioinformatics*. 2001; 45: 127–132. <https://doi.org/10.1002/prot.1171> PMID: 11835489
29. Moulton J, Fidelis K, Kryshtafovych A, Schwede T, Tramontano A. Critical assessment of methods of protein structure prediction (CASP)—Round XII. *Proteins: Structure, Function, and Bioinformatics*. 2018; 86: 7–15. <https://doi.org/10.1002/prot.25415> PMID: 29082672
30. Kryshtafovych A, Schwede T, Topf M, Fidelis K, Moulton J. Critical assessment of methods of protein structure prediction (CASP)—Round XIII. *Proteins: Structure, Function, and Bioinformatics*. 2019; 87: 1011–1020. <https://doi.org/10.1002/prot.25823> PMID: 31589781
31. Wang S, Li Z, Yu Y, Xu J. Folding Membrane Proteins by Deep Transfer Learning. *Cell Systems*. 2017; 5: 202–211.e3. <https://doi.org/10.1016/j.cels.2017.09.001> PMID: 28957654
32. Lodish H, Berk A, Zipursky SL, Matsudaira P, Baltimore D, Darnell J. *Membrane Proteins*. Molecular Cell Biology 4th edition. 2000
33. Yang J, Anishchenko I, Park H, Peng Z, Ovchinnikov S, Baker D. Improved protein structure prediction using predicted interresidue orientations. *PNAS*. 2020; 117: 1496–1503. <https://doi.org/10.1073/pnas.1914677117> PMID: 31896580
34. Heffernan R, Yang Y, Paliwal K, Zhou Y. Capturing non-local interactions by long short-term memory bidirectional recurrent neural networks for improving prediction of protein secondary structure,

- backbone angles, contact numbers and solvent accessibility. *Bioinformatics*. 2017; 33: 2842–2849. <https://doi.org/10.1093/bioinformatics/btx218> PMID: 28430949
35. Zhang C, Zheng W, Mortuza SM, Li Y, Zhang Y. DeepMSA: constructing deep multiple sequence alignment to improve contact prediction and fold-recognition for distant-homology proteins. *Bioinformatics*. 2020; 36: 2105–2112. <https://doi.org/10.1093/bioinformatics/btz863> PMID: 31738385
  36. Vassura M, Margara L, Di Lena P, Medri F, Fariselli P, Casadio R. FT-COMAR: fault tolerant three-dimensional structure reconstruction from protein contact maps. *Bioinformatics*. 2008; 24: 1313–1315. <https://doi.org/10.1093/bioinformatics/btn115> PMID: 18381401
  37. Pietal MJ, Bujnicki JM, Kozłowski LP. GDFuzz3D: a method for protein 3D structure reconstruction from contact maps, based on a non-Euclidean distance function. *Bioinformatics*. 2015; 31: 3499–3505. <https://doi.org/10.1093/bioinformatics/btv390> PMID: 26130575
  38. Kabsch W, Sander C. Dictionary of protein secondary structure: pattern recognition of hydrogen-bonded and geometrical features. *Biopolymers*. 1983; 22: 2577–2637. <https://doi.org/10.1002/bip.360221211> PMID: 6667333
  39. Zhang Y, Skolnick J. Scoring function for automated assessment of protein structure template quality. *Proteins*. 2004; 57: 702–710. <https://doi.org/10.1002/prot.20264> PMID: 15476259
  40. Xu J, Zhang Y. How significant is a protein structure similarity with TM-score = 0.5? *Bioinformatics*. 2010; 26: 889–895. <https://doi.org/10.1093/bioinformatics/btq066> PMID: 20164152
  41. Senior AW, Evans R, Jumper J, Kirkpatrick J, Sifre L, Green T, et al. Improved protein structure prediction using potentials from deep learning. *Nature*. 2020; 577: 706–710. <https://doi.org/10.1038/s41586-019-1923-7> PMID: 31942072
  42. Yıldırım MA, Goh K-I, Cusick ME, Barabási A-L, Vidal M. Drug—target network. *Nature Biotechnology*. 2007; 25: 1119–1126. <https://doi.org/10.1038/nbt1338> PMID: 17921997
  43. Huang Y, Bonett S, Kloczkowski A, Jernigan R, Wu Z. Statistical measures on residue-level protein structural properties. *J Struct Funct Genomics*. 2011; 12: 119–136. <https://doi.org/10.1007/s10969-011-9104-4> PMID: 21452025
  44. Sit A, Wu Z, Yuan Y. A Geometric Buildup Algorithm for the Solution of the Distance Geometry Problem Using Least-Squares Approximation. *Bull Math Biol*. 2009; 71: 1914. <https://doi.org/10.1007/s11538-009-9431-9> PMID: 19533250
  45. Tenenbaum JB. A Global Geometric Framework for Nonlinear Dimensionality Reduction. *Science*. 2000; 290: 2319–2323. <https://doi.org/10.1126/science.290.5500.2319> PMID: 11125149
  46. Floyd RW. Algorithm 97: Shortest Path. *Commun ACM*. 1962; 5: 345–. <https://doi.org/10.1145/367766.368168>
  47. Bhattacharya D, Cao R, Cheng J. UniCon3D: de novo protein structure prediction using united-residue conformational search via stepwise, probabilistic sampling. *Bioinformatics*. 2016; 32: 2791–2799. <https://doi.org/10.1093/bioinformatics/btw316> PMID: 27259540
  48. Torgerson WS. Multidimensional scaling: I. Theory and method. *Psychometrika*. 1952; 17: 401–419. <https://doi.org/10.1007/BF02288916>
  49. Vassura M, Margara L, Di Lena P, Medri F, Fariselli P, Casadio R. Reconstruction of 3D Structures From Protein Contact Maps. *IEEE/ACM Transactions on Computational Biology and Bioinformatics*. 2008; 5: 357–367. <https://doi.org/10.1109/TCBB.2008.27> PMID: 18670040
  50. Skwark MJ, Abdel-Rehim A, Elofsson A. PconsC: combination of direct information methods and alignments improves contact prediction. *Bioinformatics*. 2013; 29: 1815–1816. <https://doi.org/10.1093/bioinformatics/btt259> PMID: 23658418
  51. Kim DE, Chivian D, Baker D. Protein structure prediction and analysis using the Robetta server. *Nucleic Acids Res*. 2004; 32: W526–W531. <https://doi.org/10.1093/nar/gkh468> PMID: 15215442
  52. Li Y, Zhang C, Bell EW, Yu D-J, Zhang Y. Ensembling multiple raw coevolutionary features with deep residual neural networks for contact-map prediction in CASP13. *Proteins: Structure, Function, and Bioinformatics*. 2019; 87: 1082–1091. <https://doi.org/10.1002/prot.25798> PMID: 31407406
  53. Rotkiewicz P, Skolnick J. Fast procedure for reconstruction of full-atom protein models from reduced representations. *J Comput Chem*. 2008; 29: 1460–1465. <https://doi.org/10.1002/jcc.20906> PMID: 18196502